Available online at www.sciencedirect.com
SCIENCE DIRECT
Geochimica et Cosmochimica Acta 70 (2006) 965–982
Geochimica
www.elsevier.com/locate/gca

Quantification of mixing processes in ore-forming hydrothermal systems by combination of stable isotope and fluid inclusion analyses

Gregor Schwinn, Thomas Wagner *, Baldorj Baatartsogt, Gregor Markl

Institut für Geowissenschaften, Universität Tübingen, Wilhelmstrasse 56, D-72074 Tübingen, Germany

Received 17 June 2005; accepted in revised form 28 October 2005

Abstract

In the Schwarzwald area, southwest Germany, more than 400 hydrothermal veins hosting different gangue and ore mineral assemblages cross-cut the crystalline basement rocks. Many of the post-Variscan fluorite–barite–quartz veins are considered to have precipitated through mixing of a deep saline brine with meteoric, low salinity waters. This hypothesis was tested using carbon, sulfur, and oxygen isotope data of sulfides, sulfates and calcite, coupled with fluid inclusion studies. Primary hydrothermal calcites from the deposits show a positive correlation of their $\delta^{13}C$ (V-PDB) and $\delta^{18}O$ (V-SMOW) values, which range from −12 to −3‰ and from 12 to 18.5‰, respectively. Carbon and oxygen isotope compositions of paragenetically young, remobilized calcite types are shifted towards higher values and range from −12 to −1‰ and from 20 to 25‰, respectively. We developed an improved calculation procedure for modeling the covariation of carbon and oxygen isotopes in calcite resulting from mixing of two fluids with different isotopic compositions and total carbon concentrations. In our model, the carbon speciation in the two model fluid end-members and the fluid mixtures are calculated using a speciation and reaction path code. The carbon and oxygen isotope covariation of primary Schwarzwald calcites can effectively be modeled by a mixing trend of a deep saline brine and a meteoric, low salinity water. Sulfur isotope data of barites from 44 hydrothermal fluorite–barite–quartz veins vary from 9 to 18‰ (CDT), sulfide ore minerals show $\delta^{34}S$ values between −14.4 and 2.9‰. Calculated sulfide–sulfate equilibrium temperatures are in the range between 300 and 350 °C. These temperatures differ significantly from the formation temperatures of 150 to 200 °C of most of the deposits as estimated from fluid inclusions, and are interpreted as preserved paleotemperatures of the deep aquifer. This assumption has been carefully checked against possible contamination of an equilibrated sulfide–sulfate system from the deep aquifer with sulfate from surface-derived sources, considering also the kinetics of the sulfide-sulfate isotope exchange. A combination of the S isotopic results with microthermometric fluid inclusion data and constraints on the temperature of the meteoric water was used to calculate mixing ratios of the two fluid end-members. The results indicate that mass fractions of the deep saline brine in the mixed fluid were between 0.5 and 0.75. Considering all geologic, geochemical and isotopic information, we propose that the majority of the post-Variscan hydrothermal veins in the Schwarzwald area were precipitated by district-scale mixing of a homogeneous deep saline brine with meteoric waters.

1. Introduction

Fluid mixing is a widely recognized process in upper crustal hydrothermal systems (e.g., Jamtveit and Hervig, 1994; Komninou and Yardley, 1997; Gleeson et al., 2000; Douglas et al., 2003; Gleeson et al., 2003; Upton et al., 2003). Mixing of fluids with different chemical composition and/or oxidation state commonly results in supersaturation of ore and gangue minerals and occurs under conditions far from equilibrium with the host rocks (e.g., Bethke, 1996). As a consequence, fluid mixing is considered a significant precipitation mechanism involved in the formation of hydrothermal ore deposits. Many examples of Mississippi Valley-type deposits are believed to be produced by the mixing of at least two fluids (e.g., Anderson, 1975; Ohmoto and Rye, 1979; Barret and Anderson, 1982) or a metal-bearing formation water with H_2S gas (e.g., Haynes and Kesler, 1987; Jones and Kesler, 1992). Mixing between basement brines and meteoric waters accounts for the

* Corresponding author.
E-mail address: th.wagner@uni-tuebingen.de (T. Wagner).

0016-7037/$ - see front matter © 2005 Elsevier Inc. All rights reserved.
doi:10.1016/j.gca.2005.10.022

formation of many vein-type Pb–Zn mineralizations, for example within the European Variscides (e.g., Lüders and Möller, 1992; Lüders and Ebneth, 1993; Zheng and Hoefs, 1993a,b; Lüders, 1994; Ritter, 1995; Werner et al., 2000, 2002).

Stable isotope investigations of sulfur and carbon are important tools for deciphering the processes involved in the formation of hydrothermal mineralizations and can provide critical information about (1) the temperature of formation, (2) the physico-chemical conditions of the mineralization processes, and (3) the origin of the elements in solution (e.g., Rye and Ohmoto, 1974; Ohmoto and Rye, 1979; Hoefs, 1987; Rye, 1993; Ohmoto and Goldhaber, 1997; Huston, 1999; Heinrich et al., 2000; Simmons et al., 2000; Blakeman et al., 2002). In particular, sulfide–sulfate isotopic relationships are sensitive indicators for non-equilibrium assemblages resulting from fluid mixing. The isotopic exchange reaction between aqueous reduced and oxidized sulfur species is generally too slow for establishment of equilibrium fractionation during comparatively fast mineral precipitation in low- to medium-temperature hydrothermal systems (e.g., Ohmoto and Rye, 1979; Ohmoto and Lasaga, 1982). Calcites precipitated by mixing processes show carbon and oxygen isotope covariation trends controlled by the mixing ratio, the precipitation temperature and pH of the mixed fluids, and the isotopic compositions of the fluid end-members (Zheng and Hoefs, 1993c).

In this paper, we quantify fluid mixing ratios by a combination of stable isotope and fluid inclusion investigations. We propose a model for the calculation of calcite precipitation trends, which considers the isotopic composition of the fluid end-members through isotopic mass balance as well as the thermodynamically calculated carbon speciation in the mixed fluid. We show that geochemical data of many individual deposits from an area of 120 by 40 km point to large-scale hydrothermal convection and we develop a consistent model of hydrothermal mineralization via district-scale fluid mixing.

2. General geology and previous studies

2.1. General geology

In the Schwarzwald area, southwest Germany, Variscan crystalline basement rocks have been exposed during the formation of the Tertiary Rheingraben structure. The ortho- and paragneisses of the basement were intruded by granitic magmas around 335–315 Ma (Kalt et al., 2000), which form large plutons within the whole area. The western margin of the Schwarzwald is the Schwarzwald Randverwerfung fault (SRV, see Fig. 1), which separates the Rheingraben (forming part of the major Central European graben system) in the West from the Schwarzwald mountains in the East. The transitional area between the graben and the Schwarzwald mountains (Vorbergzone, see Fig. 1) contains abundant remnants of Mesozoic sedimentary rocks. In the eastern part of the Schwarzwald, the crystalline rocks are discordantly overlain by a continuous sequence of Mesozoic sediments. The lower parts of this sedimentary sequence are formed by the Lower Triassic Bunter sandstone, which are essentially sandstones and conglomerates deposited in a continental braided river system. These are followed by several marine carbonate-rich sedimentary formations ranging from Middle Triassic to late Jurassic in age. The Middle/Upper Triassic and Jurassic sediments contain abundant evaporitic units, which host significant amounts of gypsum and anhydrite. Small remnants of Paleozoic sedimentary rocks are preserved in the Badenweiler–Lenzkirch zone (BLZ, see Fig. 1), which separates the Central- from the Southern Schwarzwald. Most of the crystalline rocks of the basement show various degrees of hydrothermal alteration, with chloritization of biotite and sericitization and albitization of feldspars being the most notable alteration reactions. Entirely fresh metamorphic or igneous rocks are virtually absent in the Schwarzwald area. Oxygen isotope investigations of Hoefs and Emmermann (1983) and Simon and Hoefs (1987) demonstrate the interaction of the basement rocks with a meteoric fluid at temperatures below 500 °C. Such alteration phenomena have been dated by K–Ar and Ar–Ar studies of sericitized feldspars from the basement and the overlying Triassic Bunter sandstone at 150–110 Ma (Zuther and Brockamp, 1988; Lippolt and Kirsch, 1994; Meyer et al., 2000).

The Schwarzwald hosts an extraordinary number of hydrothermal vein-type deposits. Within an area of 120 by 40 km, more than 400 individual veins crosscut the Variscan crystalline basement and the overlying sedimentary cover. Based on their mineralogy, several hydrothermal mineralization styles can be distinguished, which are, for example, Sb–Ag-bearing quartz veins occurring throughout the entire district, Co–Ni–Ag–Bi–U-bearing barite–fluorite veins (most pronounced in the Wittichen area in the northern Schwarzwald), Fe–Mn-bearing quartz–barite veins, and Pb–(Zn)–(Ag)-bearing quartz–fluorite assemblages which are widespread in the entire southern and central Schwarzwald (Metz et al., 1957; Bliedtner and Martin, 1988).

They have been classified into (1) quartz veins, which are most probably of Variscan origin, and (2) post-Variscan fluorite–barite–quartz veins with highly variable metal assemblages. The present contribution will focus on the post-Variscan mineralizations. Most of these veins do not host minerals suitable for radiometric dating. A few measurements of pitchblende (U–Pb and U–Xe, Xe–Xe), hematite (U–He), and K-bearing minerals (K–Ar) revealed three distinct mineralization events. These are 300–240 Ma mineralizations in the Wittichen and the Menzenschwand area related to the terminal stage of the Variscan orogeny (Hofmann and Eikenberg, 1991; Meshik et al., 2000), a second one in the Hohberg and Eisenbach area at 150–110 Ma (Segev et al., 1991; Wernicke and Lippolt, 1993; Wernicke and Lippolt, 1997), and a third one at the Menzenschwand deposit at 50–30 Ma related to the formation of the Rheingraben structure (Hofmann and Eikenberg, 1991).

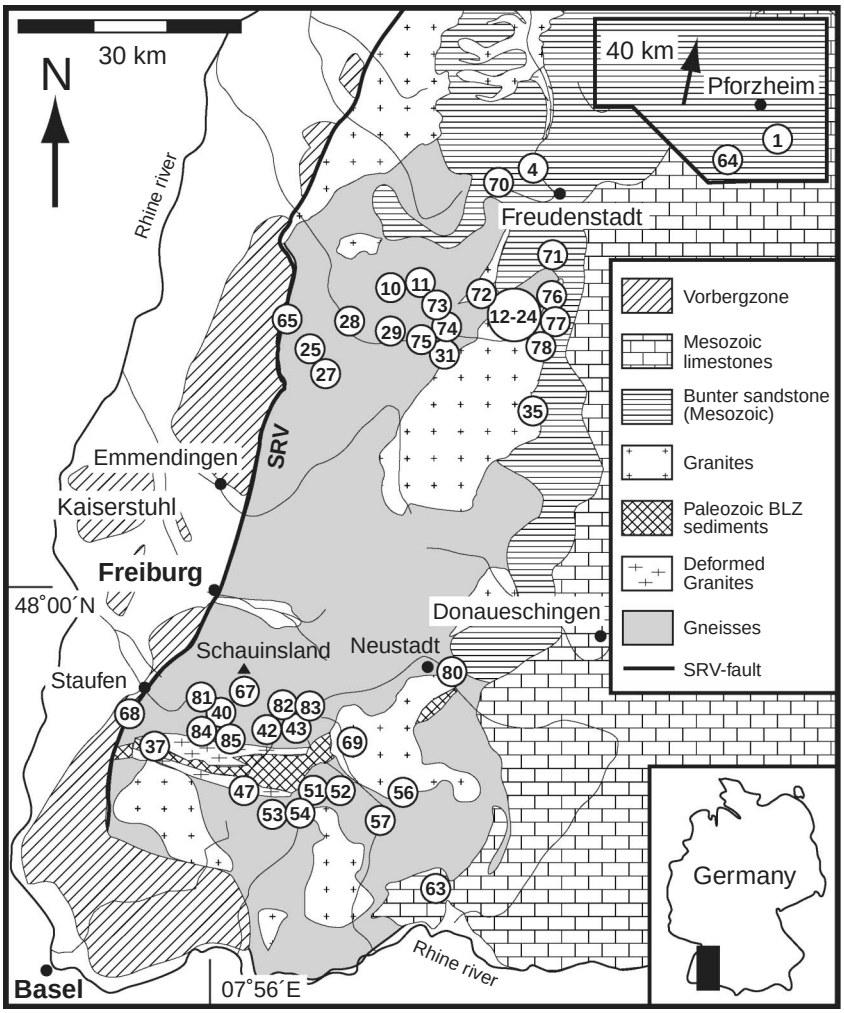

Fig. 1. Geological map of the Schwarzwald area (simpified after Metz, 1980) with the locations of the deposits. The names of the deposits correspond to the numbers in Table 1.

Most of the post-Variscan veins are oriented sub-parallel to the Rheingraben structure or they follow fracture zones which were active since late-Variscan times (Werner and Franzke, 2001). The formation of several veins parallel to the Rheingraben is believed to be related to the continuing subsidence of this structure from late Cretaceous to Tertiary times (Werner and Franzke, 2001). Within the veins, relicts of dissolved euhedral fluorite crystals and a commonly observable pseudomorphic replacement of euhedral barite crystals by quartz indicate multiple mineralization and remobilization events (Metz et al., 1957; Bliedtner and Martin, 1988). Most of the veins show a sequence of several different mineralization stages, which are (1) alteration and intense silicification of the host rocks, (2) the main barite–fluorite–quartz–calcite stage (stage I), and (3) single or multiple remobilization stages which are present as abundant fracture fillings and veinlets crosscutting the main stage mineralization (stages II and III). In addition, very late sub-recent calcite sinters can be observed in the mine workings (stage IV). The hydrothermal remobilization assemblages contain late generations of all principal gangue and ore minerals that are present in the main barite–fluorite–calcite stage mineralization. The classification of different mineralization stages used in this contribution is based on a correlation of the individual sequences found in several single veins. The observations indicate a consistent paragenetic pattern throughout the entire area. A comprehensive classification of the veins in the central and southern Schwarzwald has been presented by Bliedtner and Martin (1988) and Metz et al. (1957).

2.2. Previous studies

The results of a relatively limited sulfur isotope study of sulfide and sulfate minerals from 21 Schwarzwald deposits have been reported by von Gehlen et al. (1962). This study revealed $\delta^{34}S$ values for galena of −12.4 to −2.6‰, for sphalerite of −1.2 to 2.3‰, and for barite of 8.3–16.8‰ from different deposits. Few additional sulfur isotope data exist from deposits which are structurally related to the Tertiary Schwarzwald Randverwerfung fault. Sulfide and sulfate values from the Freiamt-Sexau mining area, Badenweiler, (Lüders, 1994) and from the Schauinsland deposit (Mittelstädt, 1987; Weber, 1997) show the same range of

$\delta^{34}S$ values as reported by von Gehlen et al. (1962). Based on these data, a qualitative fluid mixing model was proposed for the formation of the hydrothermal mineralization. This model assumes that the aqueous sulfates were derived from sulfate-bearing units of the sedimentary cover, whereas reduced sulfur originated from destruction of sulfides in metamorphic rocks of the crystalline basement (Werner et al., 2000, 2002). Variscan and post-Variscan barite types could be distinguished in the Menzenschwand mine (Hofmann, 1989), with the Variscan mineralization having distinctly lower $\delta^{34}S$ values (7.2–8.0‰) than post-Variscan barites (15.4–15.8‰). Sulfates in the Mesozoic sedimentary cover and the Tertiary sediments of the Rheingraben have been analyzed by Müller et al. (1966). The Triassic Muschelkalk and Keuper units show $\delta^{34}S$ values of 18.5–21.0 and 14.3–18.3‰, respectively. Jurassic sediments display $\delta^{34}S$ values of 16.0–19.0‰ and Tertiary units have values between 11.0 and 13.0‰.

Carbon and oxygen isotope data were reported from the Freiamt-Sexau mining area and from the Schauinsland deposit (Lüders, 1994). Two generations of siderites from Freiamt-Sexau show slight differences in their isotopic composition (generation 1: $\delta^{13}C$ of −1.7 to 2.9‰ and $\delta^{18}O$ of 17.3–17.8‰; generation 2: $\delta^{13}C$ of −3.5 to −3.2‰ and $\delta^{18}O$ of 14.6–15.5‰). In contrast, calcites from the Schauinsland mine display distinctly lower $\delta^{13}C$ and $\delta^{18}O$ values of −9 and 12‰, respectively, indicating different carbonate sources in these deposits. The $\delta^{13}C$ values of Variscan and post-Variscan calcites from the Menzenschwand mine cover a range between −10 and 0‰ and post-Variscan samples display significantly lower values than Variscan calcites (Hofmann, 1989). A single measurement of strontianite with a $\delta^{13}C$ of −5.8‰ and $\delta^{18}O$ of 20.3‰ from the Schauinsland mine is reported by Weber (1997). The $\delta^{18}O$ ratios of hydrothermal quartz from the Schwarzwald range from 12 to 18‰ (Hofmann, 1989; Weber, 1997).

As summarized above, the post-Variscan hydrothermal veins of the Schwarzwald crystalline basement show a large range of different ore and gangue mineral assemblages, and were formed through a sequence of mineralization events from late-Variscan to Tertiary times. Despite this large spectrum, fluid inclusions from almost all deposits show very similar characteristics with predominantly NaCl–$CaCl_2$-rich compositions, salinities in the range of 20–25 wt.% equivalent NaCl and homogenization temperatures of 120–180 °C (Behr and Gerler, 1987; Behr et al., 1987; von Gehlen, 1987; Werner et al., 1990; Hofmann and Eikenberg, 1991; German et al., 1994; Lippolt and Werner, 1994; Lüders, 1994; Ritter, 1995; Weber, 1997; Werner et al., 2000, 2002). Although most fluid inclusion data do not directly display mixing trends in terms of temperature–salinity correlations, many studies conclude from other paleohydrological and geochemical arguments that mixing of a high temperature, deep-sourced saline brine with cooler surface water was the dominant process responsible for vein mineralization in the Schwarzwald (von Gehlen, 1987; Behr and Gerler, 1987; Hofmann, 1989; German et al., 1994; Werner et al., 2000; Werner et al., 2002). This general view is supported by direct fluid inclusion evidence for fluid mixing, such as temperature–salinity correlations and the spatial distribution of fluid inclusion types in different zones within individual veins of the Badenweiler area (Lüders, 1994). We explain the overall fluid inclusion characteristics of the post-Variscan veins by district-scale hydrothermal convection cells which were, periodically or continuously, active since the late Permian. This assumption is supported by (1) the large-scale hydrothermal alteration of the crystalline basement, which indicates pervasive fluid flow through large portions of it (Hoefs and Emmermann, 1983; Simon and Hoefs, 1987), and (2) the similarity between REE patterns in fluorites from a large number of deposits and those in recent thermal waters from the entire Schwarzwald area (Schwinn and Markl, 2005).

3. Sampling and analytical procedures

3.1. Sampling

For this study, samples of sulfides, barite, and carbonates from 44 different post-Variscan deposits have been analyzed. The locations are shown in Fig. 1, and the names and the principal vein assemblages (main gangue minerals and characteristic metal associations) of the deposits are listed in Table 1. The deposits host various proportions of fluorite, barite, quartz, and calcite as the major vein-filling gangue minerals, which are associated with complex ore assemblages of Pb, Zn, Cu, Fe, Co, Ni, Ag, U, Bi, Sb, As, and W. For comparison, a few barren fluorite and quartz veins have been sampled as well. Most of the veins crosscut the gneisses and granites of the Variscan crystalline basement, but some deposits are hosted by sedimentary rocks. Some of the veins have been sampled in the field, and additional samples were taken from private collections and the departmental collection of the Institut für Geowissenschaften, University of Tübingen. All samples have been carefully compared with detailed textural descriptions (Metz et al., 1957; Bliedtner and Martin, 1988) to identify different mineral generations within the veins and to ensure that only cogenetic sulfide–sulfide and sulfide–sulfate mineral pairs were used for the calculation of isotopic equilibrium temperatures. Primary hydrothermal calcite I usually occurs as coarse-grained, rhombohedral calcite of white or pinkish color. The remobilized calcite generations II and III are skalenohedral crystals of white or yellow color, most frequently calcite II and III occur as euhedral crystals in vugs. Calcite IV are sub-recent calcite sinters deposited on the walls of the mine workings. In addition, samples from limestone units of the sedimentary cover and from a metamorphic calcite–prehnite–pectolite vein of Variscan age have been analyzed.

Table 1
Names of the studied deposits and hydrothermal assemblages of fluorite-bearing veins; the numbers of the deposits correspond to Fig. 1

No.	Deposit	Vein assemblage
1	Käfersteige, near Pforzheim	Fluorite–barite; Ag–Cu–Bi
4	Dorothea, near Freudenstadt	Barite–calcite; Ag–Cu
10	Clara, near Wolfach	Barite–fluorite; Cu–Ag–Pb
11	Friedrich-Christian	Fluorite–barite–quartz–calcite; Pb–Cu–Ag–Bi
12	Sophia, Wittichen	Barite–fluorite; Co–Ni–Ag–Bi–U
13	Johann, Wittichen	Barite–fluorite; Bi–Cu
21	Daniel Gallenbach, Wittichen	Fluorite–barite; Cu–Bi
25	Drey, Schnellingen	Barite–fluorite
27	Segen Gottes, Schnellingen	Barite–fluorite; Pb–Zn–Ag
28	Artenberg quarry, Steinach	Quartz–calcite–fluorite; Cu–As
31	Wenzel, near Wolfach	Barite–calcite; Ag–Sb
35	Tennenbronn, near Schramberg	Fluorite
37	Sulzburg	Fluorite
40	Teufelsgrund, Münstertal	Quartz–fluorite; Pb–Ag–Zn
42	Baumhalde, Todtnau	Quartz–fluorite; Pb–Ag–Zn
43	Brandenberg	Quartz–fluorite–(calcite); Pb–(Ag)–(Zn)–(Cu)
47	Hermann, near Görwihl	Quartz–fluorite; Pb
51	Gottes Ehre, Ruprechtgang	Quartz–fluorite–barite–calcite; Pb–Zn–Cu–Ag
52	Neuglück, Ruprechtgang	Quartz–fluorite; Pb
53	Schwarzwaldsegen, Ruprechtgang	Quartz–fluorite; Pb
54	Neuhoffnung, Ruprechtgang	Quartz–fluorite; Pb
56	Brenden	Quartz–fluorite; Pb–(Cu)
57	Igelschlatt, Schlüchttal	Quartz–fluorite; Pb–Cu–(Zn)
63	Mühlsteinbruch, near Waldshut	Quartz–(barite)–(fluorite)
64	Neubulach	Quartz–barite–calcite; Cu
65	Michael im Weiler, near Lahr	Barite; Pb–Zn
67	Schauinsland	Quartz–barite–calcite; Pb–Zn
68	Kobaltgrube, near Sulzburg	Barite–quartz–(fluorite); Co–(Ni)–Ag–Pb–Cu–(Zn)
69	Menzenschwand	Barite–fluorite–quartz; U–(Pb)–(Cu)
70	Daniel in Dehs, Bad Rippoldsau	Quartz; Cu–Ag–Bi
71	Johann Baptist, near Rippoldsau	Quartz; Cu
72	Anton im Heubach, Schiltach, Kinzigtal	Barite–fluorite; Co–Ni–Ag–Bi–U
73	Bernhard, Hauserbach	Quartz–barite–calcite; Pb–Zn–Fe
74	Maria Theresia, Hausach, Kinzigtal	Quartz–barite–calcite; Pb–Zn–Fe
75	Katharina, Trillengrund, Schiltach, Kinzigtal	Quartz–barite–calcite–(fluorite); Pb–Zn–Cu
76	Rötenbach quarry, near Alpirsbach	Calcite–dolomite; Co–Bi–Ag
77	Christiana, Wittichen	Barite–quartz; (Co)
78	Simson, Wittichen	Barite–fluorite; Co–Ni–Ag–Bi–U
80	Hammereisenbach, E Titisee-Neustadt	Barite; Fe–Mn
81	Giftgrube, Kaltwasser, Münstertal	Dolomite–calcite; Pb–As
82	Fahl, near Todtnau	Quartz–fluorite; Pb–Ag–Zn
83	Gschwend, near Todtnau	Fluorite–barite; Pb
84	Herrenwald, Münstertal	Quartz–fluorite; Pb–Ag–Zn
85	Anton, Wieden	Quartz–fluorite; Pb–Ag–Zn

3.2. Sample preparation and analytical procedures

Mineral separates of hydrothermal sulfides, sulfates, and carbonates were prepared by careful hand-picking under a binocular microscope, followed by cleaning in doubly distilled water. Sulfides and sulfates were measured after procedures given in Giesemann et al. (1994). The samples were sealed in tin capsules and converted by an EA-analyzer to SO_2 at a reaction temperature of 1050 °C and separated at a column temperature of 100 °C. The isotopic composition of SO_2 was measured with a Finnigan DeltaXL mass spectrometer. Maximum sample sizes were 0.25 mg for sphalerite and $BaSO_4$, and 0.16 mg for pyrite. Carbonate samples have been analyzed using the method of Spötl and Vennemann (2003). The isotopic composition of CO_2 was measured with a Finnigan MAT 252 mass spectrometer. The reproducibility of the isotopic ratios was ±0.1‰ for the $\delta^{13}C$ and ±0.2‰ for the $\delta^{18}O$ measurements. The reproducibility of the $\delta^{34}S$ measurements was ±0.3‰. Standards used were NBS-123 (ZnS), IAEA-S1 (AgS), IAEA-S3 (AgS), and NBS-127 ($BaSO_4$) for sulfur isotopes, and NBS-19 ($CaCO_3$) for carbon and oxygen isotopes. All sulfur, carbon and oxygen isotope compositions are reported in standard delta notation relative to V-CDT, V-PDB, and V-SMOW, respectively.

Doubly polished thin sections of fluorite, quartz, barite, and calcite have been prepared for fluid inclusion measurements from samples representative of the different mineralization stages of the veins. The microthermometric measurements were performed with a Linkam THMS-600

heating-freezing stage mounted on a Leica DMLP microscope. The calibration was done with synthetic fluid inclusions using the triple point of CO_2 (−56.6 °C), the melting point of pure H_2O (0.0 °C) and the critical point of H_2O (374.1 °C) as reference points.

4. Results

4.1. Sulfur isotopes

The results of the $\delta^{34}S$ measurements are listed in Table 2 together with equilibrium temperatures of texturally coexisting mineral pairs calculated using fractionation factors listed in Ohmoto and Goldhaber (1997). The $\delta^{34}S$ values of galena, chalcopyrite, and barite are summarized in Fig. 2. Most of the barite data range between 9 and 15‰, with only eight samples having slightly higher or lower $\delta^{34}S$ values (Fig. 2). Within individual veins, remobilized late-stage barite (Fig. 2, upside-down triangles) shows typically lower $\delta^{34}S$ values than the primary barite generation. The galena and chalcopyrite data cover a range of −14.1 to −1.6‰ and of −14.4 to 1.7‰, respectively. In the deposits Friedrich-Christian (No. 11), Brandenberg (No. 43), and Brenden (No. 56), where multiple measurements of both principal sulfide minerals could be performed, the $\delta^{34}S$ values of cogenetic galena and chalcopyrite show a relatively broad overlap (Table 2). Sphalerite and pyrite samples show distinctively higher $\delta^{34}S$ values of −3.2 to 1.5‰ and 0.8 to 2.9‰.

4.2. Carbon and oxygen isotopes

The carbon and oxygen isotope data are summarized in Tables 3 and 4; Fig. 3 displays all measurements of petrographically primary and remobilized calcites. The primary calcites show a positive correlation in $\delta^{13}C$ vs $\delta^{18}O$ space, ranging from −12.2 to −3.0‰ and from 12.0 to 18.5‰, respectively. Relatively late calcite generations within the veins display significantly higher $\delta^{13}C$ values of −12 to −1‰ and $\delta^{18}O$ values of 20–25‰. Subrecent calcite sinters (open squares) show very high $\delta^{18}O$ values around 24‰. Mesozoic Muschelkalk limestones of the sedimentary cover show relatively high $\delta^{13}C$ values of −5 to 2‰. In contrast, calcite from a metamorphic vein hosted by crystalline basement rocks and Paleozoic limestone from the Badenweiler–Lenzkirch zone have comparatively low $\delta^{13}C$ values.

5. Discussion

5.1. Sulfur isotope systematics

Equilibrium temperatures of sulfide–sulfide and sulfate–sulfide mineral pairs have been calculated using fractionation factors given in Ohmoto and Goldhaber (1997). Most interestingly, the calculated temperatures of texturally coexisting sulfide ore minerals cover a temperature range from less than 100 to 400 °C and more (Fig. 4A), whereas sulfide–sulfate temperatures show a distinct maximum of the temperature distribution around 300–350 °C (Fig. 4B). The isotopic temperatures contrast with the formation temperatures (150–200 °C) of the hydrothermal ore deposits, which are well established from fluid inclusion studies (Behr and Gerler, 1987; Behr et al., 1987; von Gehlen, 1987; Werner et al., 1990; Hofmann and Eikenberg, 1991; German et al., 1994; Lippolt and Werner, 1994; Lüders, 1994; Ritter, 1995; Weber, 1997; Werner et al., 2000; Werner et al., 2002). This indicates that ore precipitation occurred under conditions where sulfur isotope equilibrium could not be established.

We hypothesize that the temperature range of 300–350 °C calculated from sulfide–sulfate equilibria could reflect the aquifer paleotemperature of the deep saline brine, which was preserved during fluid migration. This assumption is corroborated by calculations applying the kinetic model of sulfur isotope fractionation of Ohmoto and Lasaga (1982). Assuming a near-neutral pH and a total sulfur concentration of 500–1000 ppm, the time required to establish a degree of equilibrium of 95% at 300–350 °C, i.e., at conditions prevalent in the deep fluid aquifer, is less than one year. At temperatures of 150–200 °C, which correspond to the formation temperatures of the deposits, re-establishment of the sulfide–sulfate equilibria needs 3000–7000 years. Considering the hydrodynamics of fluid migration within the fault zones, it appears plausible that fluid mixing and mineral deposition processes were too fast for re-equilibration of sulfur isotopes at formation temperatures. Relatively fast ascent of deep-sourced fluids through open fractures is consistent with the tectonic setting of the hydrothermal mineralizations in the Schwarzwald district (Franzke, 1992; Werner and Franzke, 2001).

Although the homogeneous sulfate–sulfide isotopic temperatures indicate a common deep source for both aqueous sulfate and sulfide, they do not exclude that at least part of the sulfate budget was derived from mixing with meteoric waters. Such a model has been favored by different authors for the Schauinsland deposit (Weber, 1997; Werner et al., 2002). If barite precipitation occurred as a response to instantaneous fluid mixing, the barite should then reflect the $\delta^{34}S$ value of dissolved aqueous sulfate of the meteoric fluids and fingerprint their source rocks. In this case, the observed consistent isotope temperatures would be purely coincidental. However, the sedimentary cover of the crystalline basement contains different sulfate-bearing units (Triassic to Jurassic evaporites) with very heterogeneous $\delta^{34}S$ values ranging between 12 and 21‰ (Müller et al., 1966). Considering the relatively variable $\delta^{34}S$ values of potential sulfate sources and the fact that ore-forming processes in the Schwarzwald district were operative over more than 100 Ma, we would not expect the observed narrow range of sulfate–sulfide isotope fractionation by mixing of deep brines with meteoric waters.

Table 2
Summary of the $\delta^{34}S$ values and calculated equilibrium temperatures (using fractionation factors listed in Ohmoto and Goldhaber, 1997)

No.	Deposit	Sample	Mineral	$\delta^{34}S$ (V-CDT)	Temperature (°C); sulfide pairs[a]	Temperature (°C); sulfide–sulfate[a]
1	Käfersteige (1)	BTR-30	Barite	10.7		287 (1–3)
2	Käfersteige (1)	BTR-33	Barite	17.2		208 (2–3)
3	Käfersteige (1)	BTR-34a	Chalcopyrite	−11.6		
4	Dorothea (4)	QDC-69	Barite	10.4		
5	Dorothea (4)	M-33	Chalcopyrite	−14.4		245 (3–4)
6	Friedrich-Christian (11)	GS-129	Galena	−6.4	reversed (6–7)	359 (6–8)
7	Friedrich-Christian (11)	GS-129	Chalcopyrite	−7.5		314 (7–8)
8	Friedrich-Christian (11)	GS-129	Barite	12.0		
9	Friedrich-Christian (11)	GS-118	Galena	−10.0	255 (9–10)	302 (9–8)
10	Friedrich-Christian (11)	GS-118	Chalcopyrite	−7.9		308 (10–8)
11	Friedrich-Christian (11)	MSchl-389	Galena	−5.6	>1000 (11–12)	374 (11–8)
12	Friedrich-Christian (11)	MSchl-389	Pyrite	−4.9		352 (12–8)
13	Friedrich-Christian (11)	M-3	Galena	−7.7		338 (13–8)
14	Friedrich-Christian (11)	GS-129	Galena	−8.2	156 (14-15)	328 (14–8)
15	Friedrich-Christian (11)	GS-129	Chalcopyrite	−5.1		356 (15–8)
16	Friedrich-Christian (11)	GS-142	Galena	−9.3	reversed (16–17)	312 (16–8)
17	Friedrich-Christian (11)	GS-142	Chalcopyrite	−9.7		283 (17–8)
18	Friedrich-Christian (11)	GS-135	Chalcopyrite	−7.6		313 (18–8)
19	Sophia (12)	WSB-181	Barite	13.1		
20	Sophia (12)	KL-1/63	Barite	14.2		
21	Sophia (12)	WSB-249	Barite	12.8		
22	Sophia (12)	5/97	Chalcopyrite	−1.8		401 (22–19)
23	Johann (13)	WJB-2	Chalcopyrite	−9.4		272 (23–24)
24	Johann (13)	WJB-2	Barite	13.2		
25	Johann (13)	WJB-59	Galena	−9.1	reversed (24–25)	300 (25–24)
26	Johann (13)	WJB-59	Chalcopyrite	−13.0		232 (26–24)
27	Johann (13)	910	Chalcopyrite	−12.7		234 (27–24)
28	Drey (25)	GS-151	Galena	−4.3		343 (28–29)
29	Drey (25)	GS-151	Barite	15.0		
30	Drey (25)	GS-151	Galena	−5.5		325 (30–29)
31	Drey (25)	GS-154	Galena	−5.4		326 (31–29)
32	Drey (25)	GS-151	Galena	−5.7		322 (32–29)
33	Segen Gottes (27)	XSG-20	Sphalerite	−1.9		372 (34/35–33)
34	Segen Gottes (27)	XSG-20	Barite	14.3		
35	Segen Gottes (27)	XSG-15	Barite	14.0		
36	Segen Gottes (27)	XSG-30	Chalcopyrite	−3.8	287 (35–36)	341 (34/35–36)
37	Segen Gottes (27)	BTR-3	Galena	−5.7		336 (34/35–37)
38	Artenberg (28)	XSA-66	Barite	12.4		
39	Artenberg (28)	BTR-13	Chalcopyrite	−8.4		294 (38–39)
40	Wenzel (31)	OWF-18	Barite	8.5		
41	Wenzel (31)	OWF-56	Galena	−1.6	147 (41–43)	455 (41–42)
42	Wenzel (31)	OWF-56	Barite	12.4		
43	Wenzel (31)	OWP-86	Chalcopyrite	1.6		525 (43–42)
44	Wenzel (31)	BTR-19	Galena	−1.7	143 (43–44)	453 (44–42)
45	Teufelsgrund (40)	BTR-8	Barite	20.0		
46	Teufelsgrund (40)	BTR-4	Galena	−8.3	66 (46–48)	267 (46–47)
47	Teufelsgrund (40)	BTR-4	Barite	16.7		
48	Teufelsgrund (40)	BTR-27	Chalcopyrite	−3.3		307 (48–47)
49	Teufelsgrund (40)	BTR-7	Sphalerite	−3.2		303 (49–47)
50	Teufelsgrund (40)	BTR-6	Galena	−5.4		
51	Baumhalde (42)	GS-77	Galena	−10.2		
52	Baumhalde (42)	M-ZBH-31	Galena	−14.1	65 (52–53)	
53	Baumhalde (42)	M-ZBH-31	Chalcopyrite	−9.1		
54	Baumhalde (42)	MSchl-585	Galena	−13.2	97 (53–54)	
55	Brandenberg (43)	GS-93	Galena	−8.5	89 (55–60)	284 (55–62)
56	Brandenberg (43)	GS-98	Galena	−7.0	340 (56–60)	304 (56–62)
57	Brandenberg (43)	GS-91	Galena	−8.2		288 (57–62)
58	Brandenberg (43)	MSchl-584	Galena	−5.6	reversed (58–59)	323 (58–62)
59	Brandenberg (43)	MSchl-584	Chalcopyrite	−5.7		298 (59–62)
60	Brandenberg (43)	GS-78	Chalcopyrite	−4.1		321 (60–62)
61	Brandenberg (43)	GS-86	Sphalerite	0.2		400 (61–62)
62	Brandenberg (43)	GS-86	Barite	15.0		
63	Brandenberg (43)	M"CuK/ZnS"	Sphalerite	−2.9		334 (63–62)

(*continued on next page*)

Table 2 (*continued*)

No.	Deposit	Sample	Mineral	$\delta^{34}S$ (V-CDT)	Temperature (°C); sulfide pairs[a]	Temperature (°C); sulfide–sulfate[a]
64	Brandenberg (43)	M-649	Barite	12.7		
65	Brandenberg (43)	GS-99	Barite-II	9.7		
66	Brandenberg (43)	GS-99-Sph	Sphalerite	−0.3		388 (66–62)
67	Herrmann (47)	GS-68	Galena	−2.6		600 (67–68)
68	Herrmann (47)	GS-68	Barite	8.3		
69	Gottes Ehre, Urberg (51)	M-810	Galena	−10.3	218 (69–70)	286 (69–77)
70	Gottes Ehre, Urberg (51)	M-810	Chalcopyrite	−7.9		294 (70–77)
71	Neuglück (52)	GS-26	Galena	−5.9		349 (71–77)
72	Neuglück (52)	M-UNG-9	Galena	−10.2	130 (72–73)	324 (72–77)
73	Neuglück (52)	M-UNG-9	Chalcopyrite	−6.7		320 (73–77)
74	Schwarzwaldsegen (53)	GS-28b	Galena	−7.0		330 (74–77)
75	Schwarzwaldsegen (53)	GS-28a	Galena	−8.5		309 (75–77)
76	Neuhoffnung (54)	GS-31	Galena	−10.0		288 (76–77)
77	Neuhoffnung (54)	GS-32	Barite	13.0		
78	Brenden (56)	GS-15	Galena	−10.5		303 (78–95)
79	Brenden (56)	GS-24	Galena	−11.1		295 (79–93)
80	Brenden (56)	GS-24	Galena	−11.0		295 (80–94)
81	Brenden (56)	GS-25	Galena	−9.7		315 (81–95)
82	Brenden (56)	GS-26	Galena	−9.9		313 (82–95)
83	Brenden (56)	GS-27	Galena	−10.1		309 (83–95)
84	Brenden (56)	MS-33	Galena	−11.4	380 (84–85)	292 (84–95)
85	Brenden (56)	MS-33	Chalcopyrite	−10.0		285 (85–95)
86	Brenden (56)	MS-35	Galena	−10.8	327 (86–87)	299 (86–95)
87	Brenden (56)	MS-35	Chalcopyrite	−9.3		296 (87–95)
88	Brenden (56)	MS-501	Galena	−11.6	215 (88–89)	289 (88–95)
89	Brenden (56)	MS-501	Chalcopyrite	−9.2		297 (89–95)
90	Brenden (56)	MS-564	Galena	−11.3	645 (90–91)	292 (90–95)
91	Brenden (56)	MS-564	Chalcopyrite	−10.6		278 (91–95)
92	Brenden (56)	MS-1466	Chalcopyrite	−9.0		300 (92–95)
93	Brenden (56)	GS-24	Barite	10.8		
94	Brenden (56)	GS-24	Barite	11.4		
95	Brenden (56)	GS-11	Barite	14.4		
96	Igelschlatt (57)	GS-42-2	Galena	−7.7		330 (96–102)
97	Igelschlatt (57)	GS-42-3	Galena	−8.9		312 (97–102)
98	Igelschlatt (57)	GS-42-4	Galena	−9.2		306 (98–102)
99	Igelschlatt (57)	GS-43	Galena	−8.8		315 (99–102)
100	Igelschlatt (57)	GS-57	Galena	−9.3		305 (100–102)
101	Igelschlatt (57)	GS-57	Galena	−8.0		325 (101–102)
102	Igelschlatt (57)	GS-57	Barite	13.4		
103	Igelschlatt (57)	GS-57	Barite	12.5		
104	Igelschlatt (57)	GS-45	Barite	12.3		
105	Michael im Weiler (65)	566	Galena	−4.5		355 (105–107)
106	Michael im Weiler (65)	566	Barite	14.2		
107	Michael im Weiler (65)	566	Barite	15.9		
108	Michael im Weiler (65)	782	Sphalerite	−0.1		
109	Kobaltgrube (68)	BTR-10 (Ko)	Barite	13.1		
110	Kobaltgrube (68)	DSB-29	Barite	12.9		
111	Kobaltgrube (68)	DSB-15	Galena	−4.2		382 (109/110–111)
112	Menzenschwand (69)	GMS-03	Barite	1.5		
113	Menzenschwand (69)	GMS-04	Barite	12.0		
114	Menzenschwand (69)	GMS-05	Barite	14.6		
115	Menzenschwand (69)	GMS-06	Barite	7.6		
116	Menzenschwand (69)	GMS-06	Pyrite	1.0		765 (116–114)

[a] Numbers in brackets refer to analysis numbers in column 1.

Another possible model for sulfate deposition is oxidization of aquoeus sulfide being supplied by a reduced, saline brine through mixing with meteoric water. In this case, the instantaneous oxidation and precipitation processes are too fast for establishment of isotopic equilibrium between dissolved sulfide and the aqueous sulfates formed via oxidation. The sulfide ore minerals should then display isotopic compositions very similar to barite, with only a very small fractionation between sulfide and sulfate minerals detectable (Ohmoto and Goldhaber, 1997). However, the observed sulfur isotope systematics, i.e., the consistently different $\delta^{34}S$ values of sulfides and barite from the Schwarzwald area, argues against such a model.

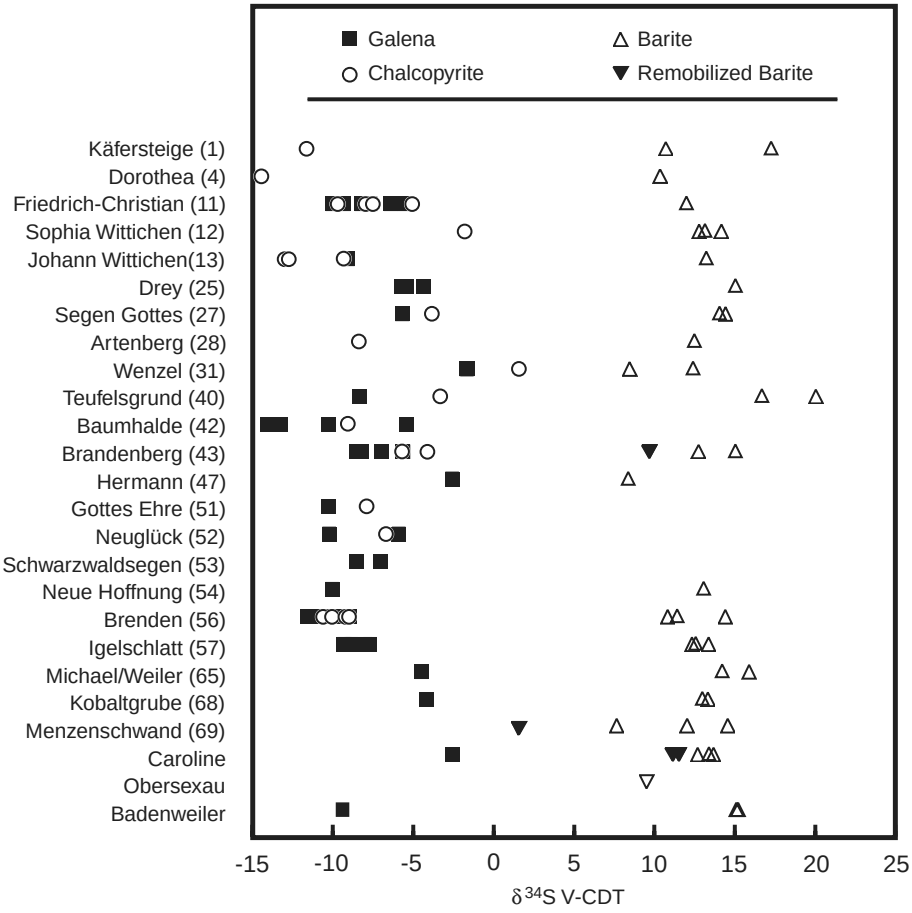

Fig. 2. Plot of the $\delta^{34}S$ values of sulfides and barite: Galena (squares), chalcopyrite (circles), barite (triangles), and remobilized barite (upside-down triangles). Data for sphalerite and pyrite are not shown.

5.2. Mixing calculations involving S isotopes

To strengthen our point, we have assessed the potential effect of contamination of a high-temperature brine transporting aqueous sulfate and sulfide in isotopic equilibrium by mixing with sulfate from meteoric water. Quantification of such a process requires reasonable estimates of the equilibrium temperatures, the sulfate concentrations and sulfur isotope composition of both end-member fluids, and the fluid mixing ratio. We know from fluid inclusion studies that the temperatures of formation of the hydrothermal vein deposits range from 150 to 200 °C at depths of around 1.5 km, and the salinities of primary fluid inclusions range from 20 to 33 wt% equivalent (eqv.) NaCl (Behr and Gerler, 1987; Behr et al., 1987; von Gehlen, 1987; Werner et al., 1990; Hofmann and Eikenberg, 1991; Lüders, 1994; Ritter, 1995; this study, Table 5). The highest salinities that were found in primary fluid inclusions of the main stage (fluorite–barite) are around 33 wt% eqv. NaCl. Considering that this fluid composition does certainly not represent the unmodified deep saline brine (prior to any mixing with meteoric water), we used an estimate of 40 wt.% eqv. NaCl for modeling. This should be very close to the true composition of the original deep-sourced brine. To make some reasonable assumptions on the paleo-hydrothermal system, we will compare the paleo-system to the recent conditions in the Schwarzwald area. This is valid because (1) the area is recently tectonically active and hosts numerous thermal springs, and (2) these thermal and mineral waters show REE patterns which are identical to patterns preserved in fluorites from the post-Variscan deposits of the Schwarzwald (Schwinn and Markl, 2005). Assuming an elevated geothermal gradient of 40 °C/km related to the intense tectonic activity of the area, the temperature of a meteoric water at 1 km depth should be close to 50 °C. Temperatures of 300 °C in the deep aquifer would be reached at depths around 7–8 km. The migrating saline brine will probably cool during the ascent from at least 7 km to the vein-forming level at 1 km depth. Hydrological data from recent geothermal wells from the Schwarzwald area show very little cooling of thermal waters during ascent on the order of 5–10 °C from 1.5 km depth (He et al., 1999). Therefore, it seems reasonable to assume cooling of the saline brine down to a temperature of about 250 °C during ascent from the deep aquifer. Using these temperature estimates for both fluid end-members, mixing calculations of a saline brine with total dissolved solutes of 40 wt% equivalent NaCl and a temperature of 250 °C with

Table 3
Summary of the carbon and oxygen isotope data of hydrothermal calcite samples from the Schwarzwald district

Deposit	Sample	Calcite stage	$\delta^{13}C$ (V-PDB)	$\delta^{18}O$ (V-SMOW)
Käfersteige	1/41	Cc II	−9.8	24.9
Käfersteige	1_BTR-30	Cc II	−9.4	24.7
Clara	10/43	Cc I	−10.3	14.3
Clara	10/44	Cc I	−9.1	15.2
Clara	10/45	Cc II	−4.9	21.5
Friedrich-Christian	11/36	Cc I	−6.1	18.2
Friedrich-Christian	11/37	Cc IV	−6.4	23.5
Friedrich-Christian	11/38	Cc I	−7.5	17.1
Friedrich-Christian	11/39	Cc II	−3.5	20.9
Friedrich-Christian	11/74	Cc IV	−1.3	23.7
Friedrich-Christian	12/54	Cc I	−10.7	15.2
Sophia	12_198	Cc II	−4.5	23.5
Sophia	12_BTR-35a	Cc II	−2.5	22.5
Sophia	12_KL-1/63	Cc I	−9.9	13.8
Sophia	12_BTR-41	Cc I	−10.8	14.9
Johann	13/8	Cc I	−10.0	15.0
Johann	13_WJB-90	Cc II	−6.0	23.7
Daniel/Gallenbach	21/2	Cc II	−7.1	17.5
Artenberg	28/55	Cc I	−8.5	13.3
Artenberg	28/56	Cc II	−9.6	15.3
Artenberg	28/57	Cc III	−11.6	24.1
Artenberg	28_BTR-13	Cc I	−10.1	13.8
Artenberg	28_XSA-47	Cc I	−11.3	11.8
Artenberg	28_XSA-47	Cc II	−11.4	24.0
Wenzel	31/19	Cc II	−10.2	21.4
Wenzel	31/33	Cc I	−8.1	14.7
Wenzel	31/34	Cc I	−11.2	14.5
Wenzel	31/50	Cc II	−6.5	21.6
Wenzel	31/51	Cc I	−12.8	13.7
Wenzel	31_BTR-18	Cc I	−11.9	13.1
Wenzel	31_BTR-18	Cc II	−6.7	20.7
Tennenbronn	35/66	Cc I	1.5	19.9
Sulzburg	37/68	Cc IV	−3.1	23.8
Teufelsgrund	40/58	Cc II	−3.5	17.2
Teufelsgrund	40/59	Cc II	−4.4	17.3
Teufelsgrund	40_BTR-5	Cc I	−4.4	17.1
Teufelsgrund	40_BTR-8	Cc I	−3.2	16.9
Brandenberg	43/60	Cc II	−3.7	17.0
Brandenberg	43/61	Cc II	−3.9	17.7
Brandenberg	43/62	Cc II	−3.7	18.3
Gottes Ehre	51/21	Cc II	−3.4	19.7
Gottes Ehre	51/22	Cc III	−6.2	21.4
Gottes Ehre	51/53	Cc I	−11.1	12.7
Mühlsandstein	63/25	Cc I	−9.0	20.1
Neubulach	64/42	Cc II	−6.5	24.1
Neubulach	64_BTR-20	Cc II	−7.2	23.9
Neubulach	64_BTR-22	Cc II	−8.0	23.8
Schauinsland	67/17	Cc I	−12.2	12.1
Schauinsland	67/18	Cc I	−12.1	12.5
Schauinsland	67/20	Cc II	−4.1	20.9
Schauinsland	67/28	Cc II	−4.5	21.3
Schauinsland	67_BTR-40	Cc I	−10.8	13.3
Daniel/Dehs	70/3	Cc I	−9.9	14.4
Daniel/Dehs	70/70	Cc II	−3.6	22.2
Daniel/Dehs	70/72	Cc I	−9.3	15.9
Johann Baptist	71/69	Cc IV	−4.6	22.2
Anton/Heubach	72/30	Cc II	−1.4	23.3
Anton/Heubach	72/73	Cc IV	0.1	24.5
Bernhard/Hauserbach	73/23	Cc II	−4.6	21.8
Bernhard/Hauserbach	73/52	Cc II	−8.0	23.2
Maria Theresia	74/47	Cc II	−4.3	21.3
Katharina/Trillengrund	75/27	Cc I	−10.4	14.6
Katharina/Trillengrund	75/75	Cc IV	−7.9	23.9
Rötenbach quarry	76/24	Cc II	−1.0	22.6
Christina/Wittichen	77/6	Cc II	−5.2	23.3
Simson/Wittichen	78/7	Cc I	−8.1	15.9
Giftgrube/Kaltwasser	81/29	Cc II	−4.3	16.5
Fahl	82/35	Cc II	−5.4	22.0
Gschwend	83/63	Cc II	−7.1	22.1
Herrenwald	84/15	Cc II or III	−3.3	15.1
Anton/Wieden	85/5	Cc II	−5.4	22.4
Wittichen area	10	Cc II or III	−2.1	21.0
Wittichen area	13	Cc II	−9.5	20.6
Wittichen area	14	Cc II	−10.8	14.4
Tunnel near Hausach	11	Cc II	−6.3	22.6
Tunnel. near Waldkirch	12	Cc II	−4.6	21.4
Randverwerfung fault	16	Cc II	−3.7	20.4
Pegmatite	46	Cc II	−6.9	23.7
Hechtsberg quarry	48	Cc II	−8.7	22.8
Hechtsberg quarry	49	Cc II	−10.2	23.8

meteoric water having a temperature of 50 °C reproduces the measured range of salinities and homogenization temperatures found in fluid inclusions (Fig. 5). The calculated mixing ratios (meteoric water/saline brine) would range between 1 and 0.33, which corresponds to mass fractions of the deep saline brine between 0.5 and 0.75.

Using these data as a basis, we can evaluate how robust the calculated sulfate–sulfide equilibrium temperatures are against meteoric contamination. Contamination of an equilibrated sulfate–sulfide system in the deep saline brine by sulfate supplied by mixing with surface-derived meteoric waters would result in a significant displacement of the calculated equilibrium temperatures. The impact of this contamination depends (1) on the mixing ratio of the two fluids, (2) on the concentrations of sulfate in the brine and the meteoric water, and (3) on the difference between the $\delta^{34}S$ values of aqueous sulfates in the brine and the meteoric source. For estimating this effect we will assume that aqueous sulfate and sulfide were equilibrated in the deep aquifer with $\delta^{34}S$ values of 13 and −9.2‰ at a temperature of 300 °C and then calculate the shift in the resulting equilibrium temperature for variations in these parameters.

To constrain the concentration ratio of aqueous sulfate in meteoric water and brine, $Rs = mSO4_{METEORIC}/mSO4_{BRINE}$, we first assume that the meteoric water is saturated with gypsum, which is, based on the abundance of sulfate-rich evaporitic series in the rock sequences through which those meteoric waters percolate, the most likely source of sulfur. Calculated sulfate concentrations at 50 °C are around 0.005 mol/kg. Crush-leach analysis of fluid inclusions from several ore deposits shows that total sulfur concentrations are around 500–1000 ppm or 0.008–0.015 mol/kg. Because the hydrothermal fluid trapped in fluid inclusions is already a mix of the deep saline brine and the meteoric water, the total sulfur concentrations in the deep saline brine were most likely even higher. Therefore, it seems reasonable to assume that the ratio *R*s is lower or equal to 0.5.

Table 4
Carbon and oxygen isotope data of calcite samples from the crystalline basement and post Variscan sedimentary rocks, Schwarzwald district

Locality	Sample	$\delta^{13}C$ (V-PDB)	$\delta^{18}O$ (V-SMOW)	Description
Urenkopf, Haslach	4	−14.4	17.0	Calcite from metamorphic prehnite–pectolite vein
Seebronn	9	−5.2	17.6	Mesozoic Muschelkalk limestone
Grimmelshofen	26	−3.1	12.3	Mesozoic Muschelkalk limestone
Niedereggenen	31	1.7	17.1	Mesozoic Muschelkalk limestone
Niedereggenen	32	1.8	18.6	Mesozoic Muschelkalk limestone
Quarry near Bernau	40	−14.5	24.4	Calcite from Paleozoic greywacke
Hammereisenbach	80/65	−8.4	24.1	Calcite from quartz–feldspar vug from pegmatite
Lierbach	64	−9.6	25.1	Calcite from agate-filled vug

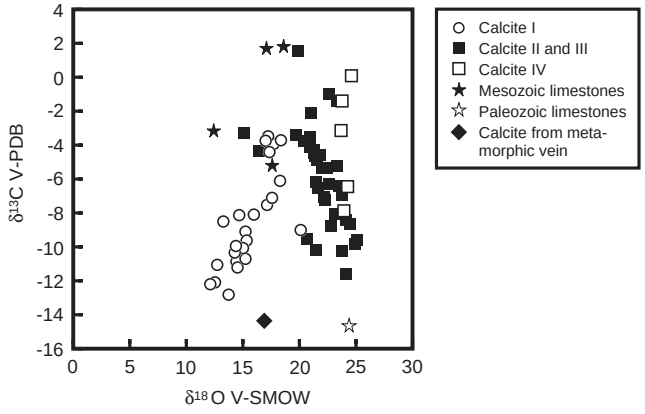

Fig. 3. Plot of the $\delta^{13}C$ and $\delta^{18}O$ values of primary hydrothermal calcites and remobilized calcites from the deposits. Open squares are very late, possibly recent sinters. Additional data are calcites from Mesozoic and Paleozoic limestones and calcite from a Variscan calcite–prehnite–pectolite vein.

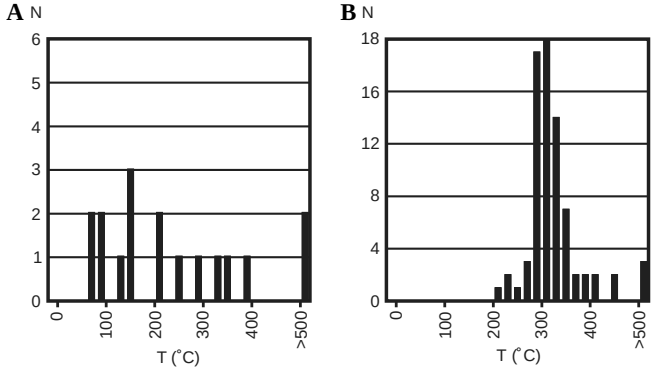

Fig. 4. Calculated sulfur isotope equilibrium temperatures for (A) sulfide–sulfide and (B) sulfide–sulfate pairs (fractionation factors from Ohmoto and Goldhaber, 1997).

Mixing with sulfate derived from Triassic sediments having a $\delta^{34}S$ value of 21‰ would have the largest effect on the resulting (in this case apparent) calculated temperatures. Fig. 6 shows mixing lines calculated for a saline brine with a $\delta^{34}S_{SULFATE}$ value of 13‰ with meteoric water with a $\delta^{34}S_{SULFATE}$ of 21‰ for a wide range of different sulfate concentration ratios *R*s. We have already estimated that the fluid mixing ratios were in the range between 0.5 and 0.75 from the reconstructed paleo-geothermal conditions

Table 5
Summary of fluid inclusion data from post-Variscan hydrothermal veins in the Schwarzwald district

Mineralization stage	Host mineral	Tm ice (°C)	Salinity (wt.%)	Th (°C)
Main stage	Fluorite	−27.0 to −20.0	22.4–26.8	120–175
	Quartz	−26.0 to −20.0	22.4–26.2	80–150
	Barite	−25.8 to −21.8	23.6–26.1	150–220
	Calcite	−28.1 to −22.0	23.7–27.5	100–180
Late stage	Fluorite	−9.4 to −1.0	1.7–13.3	120–160
	Quartz	−5.5 to −1.1	1.9–8.5	140–250
	Calcite	−5.6 to −0.2	0.4–8.7	160–200

and fluid inclusion information. A shift of the $\delta^{34}S$ value of the $\delta^{34}S_{SULFATE}$ from 13 to 14.5‰ would result in a displacement of the calculated equilibrium temperatures by about 20 °C. Any $\delta^{34}S_{SULFATE}$ of the mixed fluid which is located inside the shaded area in Fig. 6 will change the resulting equilibrium temperature by not more than 20 °C. It can be seen from Fig. 6 that a meteoric fluid at the assumed maximum sulfate concentration ratio *R*s of 0.5 could change the equilibrium temperature of the deep saline brine at mixing fractions lower than 0.7 beyond this 20 °C range. At sulfate ratios *R*s lower than 0.25, the effect on the equilibrium temperatures will be below 20 °C for all possible mixing fractions. If the isotopic composition of the sulfate in the meteoric water is lower than 21‰, even higher concentration ratios will not shift the resulting equilibrium temperatures considerably. These calculations support the idea that the observed consistent sulfate–sulfide temperatures of 300–350 °C reflect equilibrium conditions established in the deep-sourced aquifer.

5.3. Modeling of the carbon and oxygen isotope composition of mixed fluids

The measured $\delta^{13}C$ and $\delta^{18}O$ values of the primary calcites show a significant covariation, which must reflect a systematic change in the carbon and oxygen isotope composition of the hydrothermal solutions and/or temperature during progressive precipitation. To constrain the nature of this isotopic evolution, we have quantitatively modeled the isotopic effects of mixing and cooling processes. Zheng and Hoefs (1993c) have derived a two-component model to describe the covariation of $\delta^{13}C$ and $\delta^{18}O$ values of hydro-

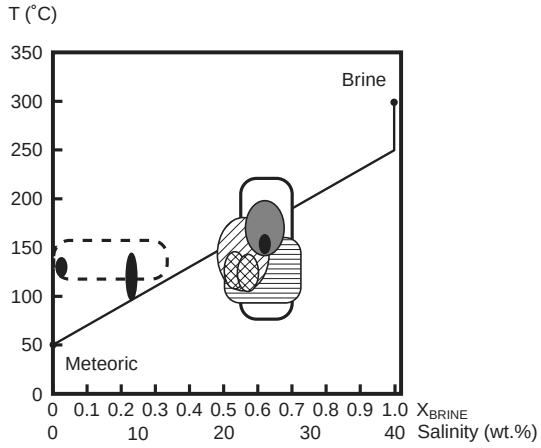

Fig. 5. Temperature of a mixed fluid plotted as a function of the mixing ratio of deep saline brine with meteoric water, and superimposed fluid inclusion data from the Schwarzwald district. Both the mass fraction of the brine and the resulting salinity (given as wt.% equivalent NaCl) are given on the abscissa. Fluid inclusion data are from Werner et al. (2000) and Mittelstädt (1987) (Schauinsland deposit, horizontal lines), Werner et al. (2000) (Teufelsgrund deposit, cross-hatched), Lüders (1994) (Badenweiler, black), Behr et al. (1987) (several post-Variscan deposits, diagonal lines), Hofmann and Eikenberg (1991) (Krunkelbach deposit, dark gray), and our data from primary fluorite, calcite, quartz, and barite (thick solid line), and late stage fluorite and calcite (thick dashed line).

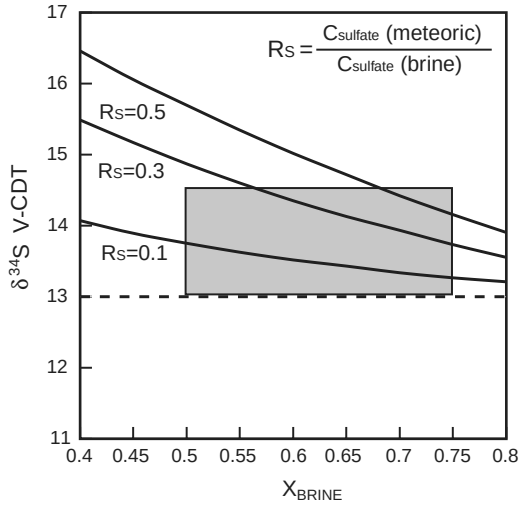

Fig. 6. Calculated mixing lines between a sulfate-bearing deep saline brine with a $\delta^{34}S$ of 13‰ and a meteoric fluid having a $\delta^{34}S$ of 21‰ at different sulfate concentration ratios *R*s. See text for explanations.

thermal calcites, which assumes mixing between a high-temperature and a low-temperature end-member fluid. Although this model has reasonably described the isotopic variation of carbonates in the Bad Grund Pb–Zn deposit (Harz Mountains, Germany), it has several limitations and simplifications, which preclude universal application to fluid mixing processes in hydrothermal systems. The model by Zheng and Hoefs (1993c) does not consider the effect of salinity on the oxygen concentration in the two fluids, which can be important for mixing between a saline brine and dilute meteoric water. The concentration of oxygen in concentrated brines with e.g., 20–40 wt.% equivalent NaCl will be much lower than in meteoric waters, and this difference has to be accounted for in the isotopic mass balance equations. Calculations assuming solute concentrations of 10 mol/kg in the brine show that this effect is about 0.2–0.3‰ per 5‰ difference in oxygen isotope composition of the two fluid end-members. For a difference of 20‰, the effect is already on the order of 1‰. Most importantly, the model by Zheng and Hoefs (1993c) assumes that the predominant aqueous carbon species in the high-temperature and low-temperature end-members are CO_2 (aq) and HCO_3^-. Mixing is then calculated as a purely physical process, ignoring the temperature and pH dependence of the CO_2–HCO_3^- equilibria.

To overcome these limitations, we have derived a modified and improved set of equations, which we have combined with calculations using a speciation and reaction path modeling code. The results of these calculations predict the aqueous carbon speciation more accurately and incorporate the effects of different starting pH values of both end-member fluids. The speciation calculations for several mixing scenarios were performed with the HCh software package (Shvarov and Bastrakov, 1999), which models heterogeneous equilibria by minimization of the Gibbs free energy of the total system (Shvarov, 1978). Thermodynamic data for aqueous species were taken from the SUPCRT92 database (Johnson et al., 1991; Shock et al., 1997; Sverjensky et al., 1997), while the thermodynamic data for solid phases came from Robie and Hemingway (1995) and Holland and Powell (1998). In the following section, we will derive the set of equations used to calculate the effect of fluid mixing on the $\delta^{13}C$ and $\delta^{18}O$ values of hydrothermal carbonates.

For mixing of two fluids having different isotope compositions, the isotopic mass balance for carbon isotopes is given by (Criss, 1999)

$$\delta^{13}C_M = X_A\delta^{13}C_A + X_B\delta^{13}C_B, \quad (1)$$

where $\delta^{13}C_A$, $\delta^{13}C_B$, and $\delta^{13}C_M$ are the carbon isotope compositions of fluids A, B, and the mixture. X_A and X_B are the mole fractions of carbon contributed from fluids A and B in the mixture. If the carbon concentrations in both fluids were identical, the mole fractions of carbon would be equal to the mole fractions of the two fluids in the mixture, f_A and f_B, where $f_B = 1 - f_A$. Now we introduce the concentration dependence in terms of molalities, and the mixing equation for carbon isotopes then becomes

$$\delta^{13}C_M = \frac{m_A f_A}{m_A f_A + m_B(1-f_A)}\delta^{13}C_A + \frac{m_B(1-f_A)}{m_A f_A + m_B(1-f_A)}\delta^{13}C_B, \quad (2)$$

where m_A and m_B are the molalities (mol/kg) of carbon in fluids A and B, respectively. However, if the salinities of both fluids are quite different, such as for mixing between a deep-sourced saline brine and dilute meteoric water, this simplified version of the mixing equation does not hold

true and has to be corrected for total solute concentrations. To accomplish this, a conversion is introduced, which relates the molalities to the total number of moles of solvent + solutes in the end-member fluids

$$m^*_A = \frac{m_A}{n_w + \sum m_{i,A}}, \quad (3)$$

where n_w is the total number of moles H_2O in 1 kg water, and $\sum m_{i,A}$ is the sum of the molalities of all solutes in fluid A. Applying these conversion factors, the mixing equation for carbon is then re-written as follows

$$\delta^{13}C_M = \frac{m^*_A f_A}{m^*_A f_A + m^*_B(1-f_A)}\delta^{13}C_A + \frac{m^*_B(1-f_A)}{m^*_A f_A + m^*_B(1-f_A)}\delta^{13}C_B. \quad (4)$$

A similar equation can be derived for oxygen isotopes, which takes into account the oxygen concentrations (corrected for total solutes) in both end-member fluids. With these equations, $\delta^{13}C$ and $\delta^{18}O$ values of the mixed fluid can be modeled. For calculating the isotopic composition of hydrothermal calcites, H_2O is the principal reservoir of oxygen, with $\delta^{18}O_{H_2O} = \delta^{18}O_M$. Consequently, only the fractionation factor between calcite (or any other carbonate mineral) and liquid H_2O at the temperature of mixing has to be applied (Ohmoto and Goldhaber, 1997).

To calculate the carbon isotope composition of calcite, the species distribution for dissolved inorganic carbon has to be considered. For geologically reasonable pH and redox conditions, CO_2 (aq) and HCO_3^- are the predominant species, whereas the concentrations of CO_3^{2-} and CH_4 (aq) are several orders of magnitude smaller. Consequently, the contribution of these species to the carbon isotope mass balance can be neglected for most cases. However, CO_3^{2-} becomes important in very alkaline solutions, so the model we present will account for all four principal species. The isotopic mass balance for the distribution of carbon isotopes between the aqueous species is given by the equation

$$\delta^{13}C_{\Sigma C} = X_{CO_2}\delta^{13}C_{CO_2} + X_{HCO_3}\delta^{13}C_{HCO_3} + X_{CO_3}\delta^{13}C_{CO_3} + X_{CH_4}\delta^{13}C_{CH_4}, \quad (5)$$

where X_{CO_2}, X_{HCO_3}, X_{CO_3}, and X_{CH_4} are the mole fractions of CO_2 (aq), HCO_3^-, CO_3^{2-}, and CH_4 (aq) in the mixed fluid, which are defined in terms of molalities. For this system, the mass balance equation for carbon takes the form $m_{\Sigma C} = m_{CO_2} + m_{HCO_3} + m_{CO_3} + m_{CH_4}$. The expressions for the isotopic fractionation factors between HCO_3^-, CO_3^{2-}, and CH_4 (aq) and CO_2 (aq) are substituted into equation (5), which is then rearranged and solved for the carbon isotope composition of CO_2 (aq)

$$\delta^{13}C_{CO_2} = \frac{\delta^{13}C_{\Sigma C} - 1000X_{HCO_3}(\alpha_{HCO_3-CO_2}-1) - 1000X_{CO_3}(\alpha_{CO_3-CO_2}-1) - 1000X_{CH_4}(\alpha_{CH_4-CO_2}-1)}{X_{CO_2} + X_{HCO_3}\alpha_{HCO_3-CO_2} + X_{CO_3}\alpha_{CO_3-CO_2} + X_{CH_4}\alpha_{CH_4-CO_2}}. \quad (6)$$

For equilibrium conditions, the isotopic composition of calcite (or any other carbonate mineral) can then be calculated from the composition of CO_2 (aq) using the equilibrium fractionation factor (Ohmoto and Goldhaber, 1997).

We have performed a number of model calculations applying the above equations, using the carbon isotope fractionation factors $\alpha_{HCO_3-CO_2}$ and α_{CAL-CO_2} from Ohmoto and Goldhaber (1997) and the oxygen isotope fractionation factor α_{CAL-H_2O} from Clayton and Kieffer (1991). Concentrations of total carbon in the two end-member fluids have been estimated by solubility calculations. The meteoric water has been saturated with calcite at a temperature of 50 °C and the system was considered to be open to the atmosphere, i.e., CO_2 and O_2 fugacities were set to atmospheric values. These calculations result in a carbon concentration of 0.00068 mol/kg in the meteoric fluid at 50 °C (Table 6). Estimations of the total carbon concentrations of the deep saline brine are more difficult. Saturation of the brine with calcite leads to rather high total carbon concentrations, which most likely do not reflect the conditions in the deep aquifer. We assumed that the pH of the hydrothermal fluid in the aquifer is primarily controlled by water-rock reactions with the crystalline host rocks and not by calcite saturation. Carbon-dissolving reactions in the aquifer, such as dissolution of carbonates and oxidation of graphite, would then not significantly modify the fluid pH. For reference, we have calculated the pH value of the saline fluid in equilibrium with a granitic assemblage, i.e., muscovite–quartz–albite–microcline, at 300–350 °C and a pressure of 1 kbar. For further calculations, we constructed a series of model fluids by adding different CO_2 concentrations and adjusting the pH back to the granite-buffered value. The most likely model setup, where calcite would be allowed to dissolve without changing the pH significantly, results in a total carbon concentration of 0.005 mol/kg (Table 6). Our model calculations show that CO_2 (aq) and HCO_3^- are by far the dominant carbon species to be considered.

Using the reconstructed model fluids, we have calculated different fluid mixing scenarios. Fig. 7 shows the relative species distribution of CO_2 (aq) and HCO_3^- during progressive mixing of the two fluids. *R*c is the concentration ratio of total dissolved carbon in both fluids, $Rc = m_{BRINE}/m_{METEORIC}$. This ratio has been estimated at around seven for the most likely case of calcite dissolution without saturation. For comparison, both 10 times higher and lower concentrations of total dissolved carbon in the brine have been considered, resulting in *R*c values of 70 and 0.7. It can be seen from Fig. 7 that the calculated speciation (solid lines) differs significantly from the ideal (physical) mixing model (dashed lines) if the concentrations

Table 6
Chemical and isotopic composition of model fluids used in mixing calculations

Parameter	Model A, meteoric	Model A, brine	Model B, meteoric	Model B, brine	Model C, meteoric	Model C, brine
T (°C)	50	350	50	350	50	350
P (bar)	Sat.	1000	Sat.	1000	Sat.	1000
pH	8.3	4.9	8.3	4.9	8.3	4.9
H_2O (kg)	1.0	1.0	1.0	1.0	1.0	1.0
CO_2 (mol)	0.00068	0.005	0.00068	0.05	0.00068	0.5
NaCl (mol)	0	7.6	0	7.6	0	7.6
KCl (mol)	0	0.62	0	0.62	0	0.62
$CaCl_2$ (mol)	0	1.7	0	1.7	0	1.7
HCl (mol)	0	0.000095	0	0	0	0
NaOH (mol)	0	0	0	0.00012	0	0.0023
$Ca(OH)_2$ (mol)	0.00015	0	0.00015	0	0.00015	0
$\delta^{13}C$ (V-PDB)	0.0	−17.0	4.0	−16.0	4.0	−16.0
$\delta^{18}O$ (V-SMOW)	−3.5	3.5	−5.0	4.0	−6.0	4.0

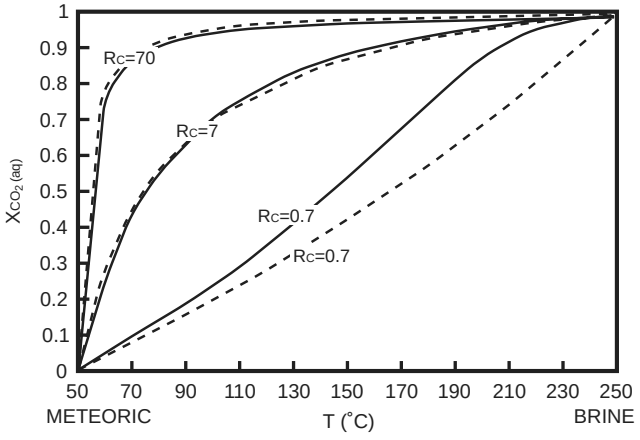

Fig. 7. Speciation of carbon given as fraction of CO_2 (aq) resulting from mixing of the two model fluid end-members at different total carbon concentration ratios *R*c. The calculated carbon speciation (solid lines) is compared with the purely physical mixing model (dashed lines).

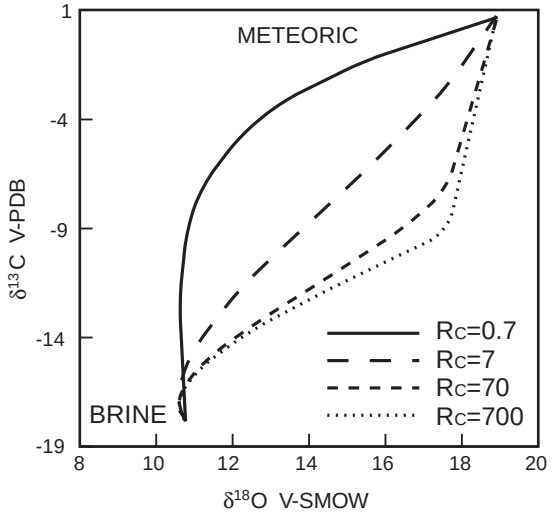

Fig. 8. Isotopic compositions of calcite precipitated via mixing of two model fluids having $\delta^{13}C = -16‰$, $\delta^{18}O = 5‰$ (deep saline brine) and $\delta^{13}C = -2‰$, $\delta^{18}O = -5‰$ (calcite-saturated meteoric fluid).

of total dissolved carbon in the high-temperature brine are equal or lower than in the low-temperature meteoric water. The ideal speciation model is reasonably consistent with the calculated speciation lines only for high values of *R*c. Fig. 8 shows the isotopic composition of calcite, precipitated from the mixing of two hypothetical fluid end-members. It was assumed that the deep saline brine has a $\delta^{13}C$ of $-16‰$ and a $\delta^{18}O$ of $5‰$, whereas the meteoric water has a $\delta^{13}C$ of $-2‰$ and a $\delta^{18}O$ of $-5‰$. It is clear that the concentration ratio *R*c has a significant effect on the curvature of the mixing line. Consequently, the measured covariation of the $\delta^{13}C$ and $\delta^{18}O$ values in the calcites contains intrinsic information, which can be used to constrain the carbon concentrations in the end-member fluids.

5.4. Carbon and oxygen isotope variation in hydrothermal calcites

To model the isotopic data of primary calcites from the Schwarzwald district, reasonable estimations of the isotopic compositions of the two fluid end-members have to be made. The selected values should reflect the isotopic compositions of the most likely sources for both fluids, as constrained by the available geological and isotopic information. The meteoric water was probably in contact with the marine limestones of the Mesozoic sedimentary units covering the crystalline basement. Surface waters from limestone aquifers typically show $\delta^{13}C$ values of -8 to $4‰$ (Ohmoto, 1986). The $\delta^{13}C$ values of granites in the Schwarzwald vary between -10 and $-26‰$ (Hoefs, 1973). Sedimentary protoliths of the gneisses will probably contain carbon originating from organic matter, which usually has $\delta^{13}C$ values of around $-25‰$ (Ohmoto and Goldhaber, 1997). Volatilization during metamorphism will lead to slight enrichment in ^{13}C compared to the sedimentary protoliths (Ohmoto, 1986). Therefore, an isotopically light composition of the carbon in the deep saline brine of around $-15‰$ or even lower can be assumed.

The $\delta^{18}O$ values of the surface-derived meteoric waters can vary along the meteoric water line from $0‰$ to negative values. Considering the paleogeography of the Schwarzwald area and modern oxygen isotopic trends in meteoric

precipitation (e.g., Bowen and Wilkinson, 2002), the original $\delta^{18}O$ values of the meteoric fluid end-member are estimated to have been in the range between −5 to 0‰. The deep saline brine is most likely of meteoric origin (Behr and Gerler, 1987; von Gehlen, 1987; Hofmann, 1989; German et al., 1994; Werner et al., 2000; Werner et al., 2002), but was extensively modified through water-rock reactions in the crystalline basement. During high-temperature water-rock interaction with crystalline rocks, the $\delta^{18}O$ of water is generally shifted towards higher values (Taylor, 1977, 1997). We have applied both closed- and open-system scenarios (Taylor, 1977, 1997) to model the isotopic exchange between water of metoric origin (with $\delta^{18}O$ between −5 and 0‰) and typical granites of the Schwarzwald area having average primary $\delta^{18}O$ values of 10‰ (Hoefs and Emmermann, 1983; Simon and Hoefs, 1987). The resulting $\delta^{18}O$ values of the deep saline brine are in the range between −1.2 and 5.3‰ for geologically reasonable water/rock ratios between 0.01 and 1.0 and an exchange temperature of 300 °C.

Table 7
Main results of the mixing calculations using model fluid compositions A, B, and C (see Table 6 for composition)

T (°C)	Model A			Model B			Model C		
	pH	HCO_3^-	CO_2 (aq)	pH	HCO_3^-	CO_2 (aq)	pH	HCO_3^-	CO_2 (aq)
250	4.6	0.0001	0.0049	4.4	0.0004	0.0495	4.2	0.0030	0.4976
240	4.6	0.0001	0.0047	4.3	0.0004	0.0471	4.2	0.0029	0.4727
230	4.6	0.0001	0.0045	4.3	0.0005	0.0446	4.1	0.0028	0.4478
220	4.6	0.0001	0.0042	4.3	0.0005	0.0421	4.0	0.0028	0.4229
210	4.7	0.0002	0.0040	4.2	0.0005	0.0396	4.0	0.0027	0.3980
200	4.7	0.0002	0.0038	4.2	0.0005	0.0371	3.9	0.0026	0.3731
190	4.7	0.0002	0.0035	4.2	0.0005	0.0347	3.9	0.0025	0.3482
180	4.8	0.0002	0.0033	4.2	0.0005	0.0322	3.8	0.0024	0.3233
170	4.8	0.0003	0.0030	4.1	0.0005	0.0297	3.8	0.0023	0.2984
160	4.9	0.0003	0.0028	4.1	0.0006	0.0272	3.7	0.0022	0.2735
150	4.9	0.0003	0.0025	4.2	0.0006	0.0248	3.7	0.0021	0.2486
140	5.0	0.0004	0.0023	4.2	0.0006	0.0223	3.7	0.0020	0.2237
130	5.0	0.0004	0.0020	4.2	0.0006	0.0198	3.7	0.0019	0.1988
120	5.1	0.0004	0.0018	4.2	0.0006	0.0173	3.7	0.0017	0.1739
110	5.2	0.0005	0.0015	4.3	0.0006	0.0148	3.7	0.0016	0.1491
100	5.3	0.0005	0.0013	4.4	0.0006	0.0124	3.8	0.0015	0.1242
90	5.4	0.0006	0.0010	4.5	0.0007	0.0099	3.8	0.0013	0.0993
80	5.6	0.0006	0.0007	4.7	0.0007	0.0074	3.9	0.0012	0.0745
70	5.8	0.0006	0.0005	4.9	0.0007	0.0049	4.1	0.0010	0.0496
60	6.2	0.0007	0.0002	5.2	0.0007	0.0025	4.3	0.0009	0.0248
50	8.1	0.0007	0.0000	8.1	0.0007	0.0000	8.1	0.0007	0.0000

Concentrations of principal aqueous carbon species are given as molalities.

Using the estimated temperatures of both end-member fluids, the modeled carbon speciation during mixing (Table 7), the concentrations of total dissolved carbon in both fluids and the likely isotopic compositions of the two fluids, the compositional range of the hydrothermal calcites can be reproduced with our mixing model (Fig. 9). The shaded areas in Fig. 9 show the likely range of isotopic compositions of the two fluids (deep saline brine and meteoric water). The isotopic compositions of the two end-member fluids used are well inside the geologically reasonable ranges. Fig. 9A has been calculated for a total carbon concentration in the deep saline brine of 0.005 mol/kg, i.e., a ratio *R*c of 7. Because a saline brine at the given temperature could possibly have even higher carbon concentrations, if calcite would be a solubility-controlling phase in the aquifer, mixing lines were also calculated using ratios of *R*c of 70 (Fig. 9B) and 700 (Fig. 9C). Fig. 9 shows that the trend of primary calcites can be well explained by the mixing of two fluids.

The compositional range of secondary or remobilized calcites can be explained by low-temperature reaction and isotopic exchange with meteoric waters. Remobilization of calcite having a $\delta^{13}C$ of about −2‰ through interaction with a bicarbonate-dominated meteoric water at temperatures around 50 °C will shift the $\delta^{13}C$ value of precipitating secondary calcites to −0.3‰. Assuming a $\delta^{18}O$ value of roughly 0‰ for the meteoric water, the remobilization will

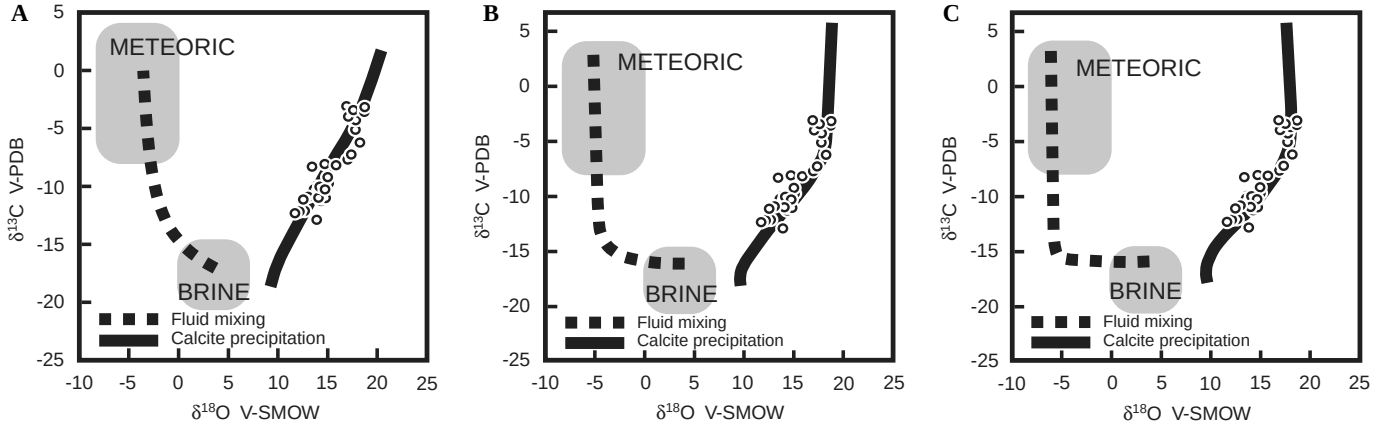

Fig. 9. Plot of the $\delta^{13}C$–$\delta^{18}O$ covariation of primary hydrothermal calcites from the Schwarzwald district compared to the results of the fluid mixing calculations. The shaded areas indicate the likely range of isotopic compositions of the two fluids, constrained by the isotopic data of geologically reasonable fluid sources in the literature. The dashed lines show the mixing trends for the fluids, whereas the solid lines indicate the isotopic compositions of the corresponding calcites, precipitated from the mixed fluid. (A) *R*c = 7, (B) *R*c = 70, (C) and *R*c = 700.

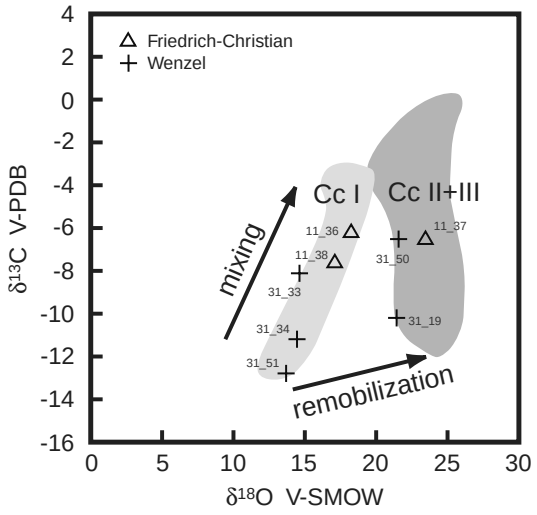

Fig. 10. Binary diagram of the $\delta^{13}C$ and $\delta^{18}O$ values of primary and remobilized hydrothermal calcites, showing the principal mixing and remobilization trends.

result in $\delta^{18}O$ values of the secondary calcites of around 24‰. The remobilization trend indicated in Fig. 10 shows that the direction of this shift is quite distinct from the primary calcite trend. Individual measurements of different calcite generations from the Friedrich-Christian (No. 11) and Wenzel (No. 31) deposits substantiate the remobilization model (Fig. 10). The low-temperature remobilization can explain that the isotopic compositions of all secondary calcites are shifted towards higher $\delta^{13}C$ and $\delta^{18}O$ values, compared to the primary hydrothermal calcites.

6. Conclusions

Consistent sulfide–sulfate equilibrium temperatures of about 300 °C from several locations within the entire Schwarzwald district demonstrate the existence of a large homogeneous fluid reservoir at around 7–10 km depth. Integration of several datasets including fluid inclusion salinities, deposit formation temperatures, and calculated aquifer temperatures is used to derive a model of district-scale fluid mixing between a deep saline brine and surface-derived meteoric waters. Calculations indicate that mass fractions of the high-salinity end-member were on the order of 0.5–0.75.

The isotopic compositions of hydrothermal calcites precipitated via mixing of the two fluids have been modeled by a combination of isotopic mass balance equations and speciation calculations. Geologically reasonable estimates for the isotopic compositions of the two fluid end-members have been integrated into the model, permitting reconstruction of paleo-mixing-lines that reproduce the measured covariation of $\delta^{13}C$ and $\delta^{18}O$ of the calcites. This confirms that mixing of homogeneous deep saline brines with surface-derived meteoric water was a large-scale process responsible for the formation of most hydrothermal ore deposits in the Schwarzwald district. The many similar geochemical characteristics, such as salinities and compositions of fluids, homogenization temperatures of fluid inclusions, stable isotope compositions of oxygen, sulfur, and carbon, REE pattern of fluorites (Schwinn and Markl, 2005), of the hydrothermal deposits over a large area are attributed to this large-scale convection system.

Most likely, this hydrothermal system has been active from Mesozoic to recent times. A major Jurassic alteration event which affected the crystalline basement and the Triassic sedimentary cover (Zuther and Brockamp, 1988; Lippolt and Kirsch, 1994; Meyer et al., 2000) demonstrates the deep migration of a meteoric fluid, possibly seawater, into the crust. This fluid was extensively modified by water-rock interaction and stored as deep saline groundwater in the crystalline basement. The chemical compositions of recent thermal waters, which originate from several km deep reservoirs, show a fossil seawater component (He et al., 1999; Stober and Bucher, 1999; Stober et al., 1999). During times of increased tectonic activity, pathways allowed the ascent of this brine to the subsurface (Werner et al., 2002), and mixing with shallow meteoric waters as proposed in the model of the present study lead to the formation of the post-Variscan fluorite–barite–quartz veins of the Schwarzwald district.

Acknowledgments

This project was made possible by funding from the German Research Council (DFG) to G.M. We thank three anonymous reviewers for their constructive comments, and the guidance of Edward Ripley which were most helpful for improving the paper.

Associate editor: Edward M. Ripley

References

Anderson, G.M., 1975. Precipitation of Mississippi valley-type ores. *Econ. Geol.* **70**, 937–942.

Barret, T.J., Anderson, G.M., 1982. The solubility of sphalerite and galena in NaCl brines. *Econ. Geol.* **77**, 1923–1933.

Behr, H.J., Gerler, J., 1987. Inclusions of sedimentary brines in post-Variscan mineralizations in the Federal Republic of Germany—a study by neutron activation analysis. *Chem. Geol.* **61**, 65–77.

Behr, H.J., Horn, E.E., Frenzel-Beyme, K., Reutel, C., 1987. Fluid inclusion characteristics of the Variscan and post-Variscan mineralizing fluids in the Federal Republic of Germany. *Chem. Geol.* **61**, 273–285.

Bethke, C.M., 1996. *Geochemical Reaction Modelling*. Oxford University Press, New York.

Blakeman, R.J., Ashton, J.H., Boyce, A.J., Fallick, A.E., Russell, M.J., 2002. Timing of interplay between hydrothermal and surface fluids in the Navan ZnPb orebody, Ireland: evidence from metal distribution trends, mineral textures, and $\delta^{34}S$ analyses. *Econ. Geol.* **97**, 73–91.

Bliedtner, M., Martin, M., 1988. *Erz- und Minerallagerstätten des Mittleren Schwarzwaldes*. Geologisches Landesamt Baden-Wuerttemberg, Freiburg i.Br.

Bowen, G.J., Wilkinson, B., 2002. Spatial distribution of $\delta^{18}O$ in meteoric precipitation. *Geology* **30**, 315–318.

Clayton, R.N., Kieffer, S.W., 1991. Oxygen isotopic thermometer calibrations. In: Taylor, H.P., O'Neil, J.R., Kaplan, I.R. (Eds.). Isotope Geochemistry: A Tribute to Samuel Epstein Geochem. Soc. Spec. Publ. 3, pp. 3–10.

Criss, R.E., 1999. *Principles of Stable Isotope Distribution*. Oxford University Press, New York-Oxford, p. 264.

Douglas, T.A., Chamberlain, C.P., Poage, M.A., Abruzzese, M., Shultz, S., 2003. Fluid flow and the Heart Mountain fault: a stable isotopic, fluid inclusion, and geochronologic study. *Geofluids* **3**, 13–32.

Franzke, H.J., 1992. Die strukturelle Enwicklung mineralisierter Störungszonen im Schwarzwald. Unpublished technical report, GFZ-Postdam, Germany.

von Gehlen, K., Nielsen, H., Ricke, W., 1962. S-Isotopen Verhältnisse in Baryt und Sulfiden aus hydrothermalen Gängen im Schwarzwald und jüngeren Barytgängen in Süddeutschland und ihre genetische Bedeutung. *Geochim. Cosmochim. Acta* **26**, 1189–1207.

von Gehlen, K., 1987. Formation of Pb–Zn–F–Ba mineralizations in SW Germany: a status report. *Fortschritte der Mineralogie* **65**, 87–113.

German, A., Lang, R., Werner, W., Friedrich, G., 1994. Zur Mineralogie und Geochemie der Erzgänge im Bergbaurevier Freiamt-Sexau, Mittlerer Schwarzwald. In: Storch, D.H., Werner, W. (Eds.), Die Erz- und Mineralgänge im alten Bergbaurevier "Freiamt-Sexau, Mittlerer SchwarzwaldAbh. Geol. Landesamt Baden-Württemberg, vol. 14, pp. 119–155.

Giesemann, A., Jäger, H., Norman, A., Brand, W., 1994. On-line sulfur isotope determination using an element analyzer coupled to mass spectrometer. *Anal. Chem.* **66**, 2816–2819.

Gleeson, S.A., Yardley, B.W.D., Munz, I.A., Boyce, A.J., 2003. Infiltration of basinal fluids into high-grade basement, South Norway: Sources and behaviour of waters and brines. *Geofluids* **3**, 33–48.

Gleeson, S.A., Yardley, B.W.D., Boyce, A.J., Fallick, A.E., Munz, I.A., 2000. From basin to the basement: the movement of surface fluids into the crust. *J. Geochem. Explor.* **69-70**, 527–531.

Haynes, F.M., Kesler, S.E., 1987. Chemical evolution of brines during Mississippi Valley-type mineralization: evidence from East Tennessee and Pine Point. *Econ. Geol.* **82**, 53–71.

He, K., Stober, I., Bucher, K., 1999. Chemical evolution of thermal waters from limestone aquifers of the Southern Upper Rhine Valley. *Appl. Geochem.* **14**, 223–235.

Heinrich, C.A., Andrew, A.S., Knill, M.D., 2000. Regional metamorphism and ore formation: evidence from stable isotopes and other fluid tracers. *Rev. Econ. Geol.* **11**, 97–117.

Hoefs, J., 1973. Ein Beitrag zur Isotopengeochemie des Kohlenstoffs in magmatischen Gesteinen. *Contrib. Mineral. Petrol.* **41**, 277–300.

Hoefs, J., 1987. *Stable Isotope Geochemistry*, third ed. Springer, Berlin Heidelberg New-York, p. 241.

Hoefs, J., Emmermann, R., 1983. The oxygen isotope composition of Hercynian granites and pre-Hercynian gneisses from the Schwarzwald, SW Germany. *Contrib. Mineral. Petrol.* **83**, 320–329.

Hofmann, B., 1989. Genese, Alteration und rezentes Fliesssystem der Uran-Lagerstätte Krunkelbach, Menzenschwand, Südschwarzwald. Technical Report 88-30, Mineralogisch-Petrographisches Institut, University of Bern, Switzerland.

Hofmann, B., Eikenberg, J., 1991. The Krunkelbach uranium deposit, Schwarzwald, Germany. Correlation of radiometric ages, U–Pb, U–Xe–Kr, K–Ar, Th–U with mineralogical stages and fluid inclusions. *Econ. Geol.* **86**, 1031–1049.

Holland, T.J.B., Powell, R., 1998. An internally consistent thermodynamic data set for phases of petrological interest. *J. Metamorph. Geol.* **16**, 309–343.

Huston, D.L., 1999. Stable isotopes and their significance for understanding the genesis of volcanic-hosted massive sulfide deposits: a review. *Rev. Econ. Geol.* **8**, 157–179.

Jamtveit, B., Hervig, R.L., 1994. Constraints on transport and kinetics in hydrothermal systems from zoned garnet crystals. *Science* **263**, 505–508.

Johnson, J.W., Oelkers, E.H., Helgeson, H.C., 1991. SUPCRT92, a software package for calculating the standard molal thermodynamic properties of minerals, gases, aqueous species, and reactions from 1 to 5000 bars and 0 to 1000 °C. *Comput. Geosci.* **18**, 899–947.

Jones, H.D., Kesler, S.E., 1992. Fluid inclusion gas chemistry in East Tennessee Mississippi Valley-type districts; evidence for immiscibility and implications for depositional mechanisms. *Geochim. Cosmochim. Acta* **56**, 137–154.

Kalt, A., Altherr, R., Hanel, M., 2000. The Variscan Basement of the Schwarzwald. Eur. J. Mineral. 12 (Beih.2.) 1–43.

Komninou, A., Yardley, B.W.D, 1997. Fuid-rock interaction in the Rhine Graben: a thermodynamic model of the hydrothermal alteration observed in deep drilling. *Geochim. Cosmochim. Acta* **61**, 515–531.

Lippolt, H.J., Werner, O., 1994. Die genetische Aussage von Blei-Isotopen-Verhältnissen in Bleiglanzen des Bergbaureviers Freiamt-Sexau, Mittlerer Schwarzwald. In: Storch, D.H., Werner, W. (Eds), Die Erz-und Mineralgänge im alten Bergbaurevier "Freiamt-Sexau, Mittlerer Schwarzwald Abh. Geol. Landesamt Baden-Württemberg, vol. 14, pp. 191–205.

Lippolt, H.J., Kirsch, H., 1994. Isotopic investigation of post-Variscan Plagioclase Sericitization in the Schwarzwald Gneiss Massif. *Chem. Erde* **54**, 179–198.

Lüders, V., 1994. Geochemische Untersuchungen an Gangartmineralen aus dem Bergbaurevier Freiamt-Sexau und dem Badenweiler-Quarzriff, Schwarzwald. In: Storch, D.H., Werner, W. (Eds.), Die Erz-und Mineralgänge im alten Bergbaurevier "Freiamt-Sexau, Mittlerer SchwarzwaldAbh. Geol. Landesamt Baden-Württemberg, vol. 14, pp. 173–191.

Lüders, V., Ebneth, J., 1993. Sulfur isotopes in shales and their relation to vein sulfides (and barite) of the Upper and Middle Harz Mountains. *Monogr. Ser. Miner. Deposits* **30**, 231–240.

Lüders, V., Möller, P., 1992. Fluid evolution and ore deposition in the Harz Mountains (Germany). *Eur. J. Miner.* **4**, 1053–1068.

Meshik, A.P., Lippolt, H.J., Dymkov, Y.M., 2000. Xenon geochronology of Schwarzwald pitchblendes. *Miner. Deposita* **35**, 190–205.

Metz, R., 1980. Geologische Landeskunde des Hotzenwaldes. Moritz Schauenburg Verlag, Lahr/Schwarzwald.

Metz, R., Richter, M., Schürenberg, H., 1957. Die Blei-Zink-Erzgänge des Schwarzwaldes. *Beih. Geol. Jahrb.* **29**, 1–277.

Meyer, M., Brockamp, O., Clauer, N., Renk, A., Zuther, M., 2000. Further evidence for a Jurassic mineralizing event in central Europe. K–Ar dating of geothermal alteration and fluid inclusion systematics in wall rocks of the Käferteige fluorite vein deposit in the northern Black Forest, Germany. *Miner. Deposita* **35**, 754–761.

Mittelstädt, R., 1987. Flüssigkeitseinschluss-und Isotopenuntersuchungen an Mineralen der Blei Zink-Lagerstätte Schauinsland im südlichen Schwarzwald. Diploma thesis, University of Göttingen, Germany.

Müller, G., Nielsen, H., Ricke, W., 1966. Schwefel-Isotopen-Verhältnisse in Formationswässern und Evaporiten Nord- und Süddeutschlands. *Chem. Geol.* **1**, 211–220.

Ohmoto, H., 1986. Stable isotope geochemistry of ore deposits. In: Valley, J.W., Taylor, H.P., O'Neil, J.R. (Eds.), Stable Isotopes in High-Temperature Geological Processes. Rev. Mineral. 16, pp. 491–559.

Ohmoto, H., Rye, R.O., 1979. Isotopes of sulfur and carbon. In: Barnes, H.L. (Ed.), *Geochemistry of Hydrothermal Ore Deposits*, second ed. Wiley, New York, pp. 505–567.

Ohmoto, H., Lasaga, A.C., 1982. Kinetics of reactions between aqueous sulfates and sulfides in hydrothermals systems. *Geochim. Cosmochim. Acta* **46**, 1727–1745.

Ohmoto, H., Goldhaber, M.B., 1997. Sulfur and carbon isotopes. In: Barnes, H.L. (Ed.), *Geochemistry of Hydrothermal Ore Deposits*, third ed. Wiley, New York, pp. 517–611.

Ritter, J., 1995. Genese der Mineralistation Herrmanngang im Albtalgranit, SE-Schwarzwald und Wechselwirkungen mit dem Nebengestein. *Karlsruher Geochemische Hefte* **8**, 1–132.

Robie, R.A., Hemingway, B.S., 1995. Thermodynamic properties of minerals and related substances at 298.15 K and 1 Bar (105 Pascals) pressure and at higher temperatures. U.S. Geol. Surv. Bull. 2131, p. 461.

Rye, R.O., 1993. The evolution of magmatic fluids in the epithermal environment: the stable isotope perspective. *Econ. Geol.* **88**, 733–753.

Rye, R.O., Ohmoto, H., 1974. Sulfur and carbon isotopes and ore genesis: a review. *Econ. Geol.* **69**, 826–842.

Schwinn, G., Markl, G., 2005. REE systematics in hydrothermal fluorite. *Chem. Geol.* **216**, 225–248.

Segev, A., Halicz, L., Lang, B., Steinitz, G., 1991. K-Ar dating of manganese minerals from the Eisenbach region, Black Forest, southwest Germany. *Schweiz. Miner. Petrogr. Mitt.* **71**, 101–114.

Shock, E.L., Sassani, D.C., Willis, M., Sverjensky, D.A., 1997. Inorganic species in geological fluids: correlations among standard molal thermodynamic properties of aqueous ions and hydroxide complexes. *Geochim. Cosmochim. Acta* **61**, 907–950.

Shvarov, Y.V., 1978. Minimization of the thermodynamic potential of an open chemical system. *Geochem. Internat.* **15**, 200–203.

Shvarov, Y.V., Bastrakov, E., 1999. HCh: a software package for geochemical equilibrium modeling. User's guide. Australian Geological Survey Organisation, Department of Industry, Science and Resources.

Simmons, S.F., Arehart, G.B., Simpson, M.P., Mark, J.L., 2000. Origin of massive calcite veins in the golden cross low-sulfidation epithermal Au–Ag deposit, New Zealand. *Econ. Geol.* **95**, 99–112.

Simon, K., Hoefs, J., 1987. Effects of meteoric water interaction on Hercinian granites from the Südschwarzwald, southwest Germany. *Chem. Geol.* **61**, 253–261.

Spötl, C., Vennemann, T.W., 2003. Continuous-flow isotope ratio mass spectrometric analysis of carbonate minerals. *Rapid. Commun. Mass. Spectrom.* **17**, 1004–1006.

Stober, I., Bucher, K., 1999. Deep groundwater in the crystalline basement of the Black Forest region. *Appl. Geochem.* **14**, 237–254.

Stober, I., Richter, A., Brost, E., Bucher, K., 1999. The Ohlsbach plume—discharge of deep saline water from the crystalline basement of the Black Forest, Germany. *Hydrogeol. J.* **7**, 273–283.

Sverjensky, D.A., Shock, E.L., Helgeson, H.C., 1997. Prediction of the thermodynamic properties of aqueous metal complexes to 1000 °C and 5 kb. *Geochim. Cosmochim. Acta* **61**, 1359–1412.

Taylor Jr., H.P., 1977. Water/rock interactions and the origin of H_2O in granitic batholiths. *J. Geol. Soc. Lond.* **133**, 509–558.

Taylor, H.P., 1997. Oxygen and hydrogen isotope relationships in hydrothermal mineral deposits. In: Barnes, H.L. (Ed.), *Geochemistry of Hydrothermal Ore Deposits*, third ed. Wiley, New York, pp. 229–302.

Upton, P., Craw, D., Caldwell, T.G., Koons, P.O., James, Z., Wannamaker, P.E., Jiracek, G.J., Chamberlain, C.P., 2003. Upper crustal fluid flow in the outboard region of the Southern Alps, New Zealand. *Geofluids* **3**, 1–12.

Weber, A., 1997. Geochemische Untersuchungen zur Genese der Blei-Zink-Lagerstätte am Schauinsland im Schwarzwald. Diploma thesis, Faculty of Geosciences, University of Tübingen, Germany.

Werner, W., Franzke, H.J., Wirsing, G., Jochum, J., Lüders, V., Wittenbrink, J., 2002. Die Erzlagerstätte Schauinsland bei Freiburg im Breisgau. Aedificatio Verlag, Freiburg.

Werner, W., Franzke, H.J., 2001. Postvariskische bis neogene Bruchtektonik und Mineralisation im südlichen Schwarzwald. *Z. Dt. Geol. Ges.* **152**, 405–437.

Werner, W., Franzke, H.J., Lüders, V., 2000. Zur Genese der Zink-Blei-Lagerstätte Schauinsland. *Erzmetall* **53**, 273–285.

Werner, W., Schlaegel-Blaut, P., Rieken, R., 1990. Verbreitung und Ausbildung von Wolframmineralisationen im Kristallin des Schwarzwaldes. *Jh. Geol. Landesamt Baden-Württemberg* **32**, 17–61.

Wernicke, R.S., Lippolt, H.J., 1993. Botryoidal hematite from the Schwarzwald, Germany. Heterogenous U distributions and their bearing on the helium dating method. *Earth Planet. Sci. Lett.* **114**, 287–300.

Wernicke, R.S., Lippolt, H.J., 1997. U–Th–He evidence of a Jurassic continuous hydrothermal activity in the Schwarzwald basement, Germany. *Chem. Geol.* **138**, 273–285.

Zheng, Y.F., Hoefs, J., 1993a. Stable isotope geochemistry of hydrothermal mineralizations in the Harz Mountains: I. Carbon and oxygen isotopes of carbonates and implications for the origin of hydrothermal fluids. *Monogr. Ser. Miner. Deposits* **30**, 169–187.

Zheng, Y.F., Hoefs, J., 1993b. Stable isotope geochemistry of hydrothermal mineralizations in the Harz Mountains: II.Sufur and oxygen isotopes of sulfides and sulfate and constraints on metallogenic models. *Monogr. Ser. Miner. Deposits* **30**, 211–229.

Zheng, Y.F., Hoefs, J., 1993c. Carbon and oxygen isotopic covariations in hydrothermal calcites. Theoretical modeling on mixing processes and application to Pb–Zn deposits in the Harz Mountains, Germany. *Miner. Deposita* **28**, 79–89.

Zuther, M., Brockamp, O., 1988. The fossil geothermal system of the Baden-Baden trough, northern Black Forest, Germany. *Chem. Geol.* **71**, 337–353.